Geomorphology 466 (2024) 109434

Contents lists available at ScienceDirect

Geomorphology

journal homepage: www.journals.elsevier.com/geomorphology

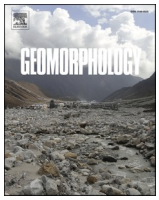

# Imprint of a dead-ice environment on lidar imagery—Spatial patterns at the last Scandinavian Ice Sheet margin (N Poland)

Barbara Woronko [a,*], Weronika Danel [b], Mirosław Błaszkiewicz [c], Piotr Hermanowski [d], Olaf Juschus [e], Mateusz Kramkowski [c], Bruno Garrett [c], Achim Brauer [f]

[a] Faculty of Geology, University of Warsaw, Warsaw, Poland
[b] Polish Geological Institute – National Research Institute, Warsaw, Poland
[c] Institute of Geography and Spatial Organization of the Polish Academy of Science, Department of Environmental Resources and Geohazards, Poland
[d] Institute of Geology, Adam Mickiewicz University, Poznań, Poland
[e] State Office for Mining, Geology and Raw Materials Brandenburg, Department 22, Cottbus, Germany
[f] GFZ –German Research Centre for Geosciences, Section Climate Dynamics and Landscape Evolution, Potsdam, Germany

ARTICLE INFO

*Keywords:*
Ridges surrounding pits
Morphometry
Digital elevation model (DEM)
Glacial topography
ZMP ridges and pits

ABSTRACT

There is a unique glacial landscape system in the southern Żarnowiec Moraine Plateau of northern Poland. Here the terrain is characterized by a very high concentration of ridges that are often adjacent to pits, which together constitutes a special type of hummocky topography. The morphological diversity of the study-area ridges and pits was determined from high-resolution lidar imagery that was qualitatively and quantitatively processed, then analysed. Fourteen test fields of spatial dimensions 0.5 km × 0.5 km were selected within the moraine plateau for detailed studies. The results show that the ridges and pits constitute a very dense network of approximately circular, diverse-oriented forms of various sizes, most of which are linked to each other in a step-wise fashion. The pits are surrounded by ridges of various heights and widths that separate one pit from another. A characteristic feature of the studied pits is the orientation of their long axis. Form-based morphological analysis revealed that their genesis was associated with a glacial rather than a periglacial environment. It is believed that ridge orientation reflects a spatial pattern related to ice crevasses. A moraine plateau constituted a terrain obstacle that acted as a counterslope to the advancing ice sheet. The studied landforms and landscape resulted from the ice sheet's breaking up into dead-ice blocks of various sizes. The very dense system of perpendicular, parallel, and diagonal crevasses was related to ice sheet advance from a northerly direction, resulting in a flow around the obstacle and differences in ice-mass speed.

## 1. Introduction

A digital elevation model (DEM) of extraordinary resolution based on airborne LiDAR (Light Detection And Ranging), whose laser beam has the capacity to penetrate through gaps in vegetation (Höfle et al., 2009), enable not only an extremely precise analyses of landscape relief and morphometric characteristics of forms (Ojala et al., 2019; Sookhan et al., 2021; Adamczyk et al., 2022; Łopuch et al., 2023; Szuman et al., 2023) and a reinterpretation of existing views on the evolution of the relief (Łopuch et al., 2023), but also the discovery of new glacial landforms that have been impossible to identify using traditional tools-including triangular-shaped hummocks (murtoos) (Ojala et al., 2019, 2021; Peterson and Johnson, 2021), glacial curvilineations within tunnel valley (Adamczyk et al., 2022), and post-glacial surface cracks (Karasiewicz et al., 2023). Therefore, DEMs have a very wide application in geomorphology and geology, and further utility extending into other sciences such as archaeology (e.g., Štular et al., 2021).

The marginal zone of the Pleistocene ice sheets is usually characterized by the topographically complex landscape formed due to stagnant-ice melting. This type of landscape is commonly referred to as dead-ice moraine, stagnation moraine, or hummocky moraine (Clayton and Moran, 1974; Eyles et al., 1999; Boone and Eyles, 2001). Among them, landforms of a roughly circular shape can be distinguished. These forms of variable size are elongated or circular ridges, which are often surrounded by a peat-filled basin. They are not solitary landforms but occur in groups or clusters. Forms of this type are usually non-oriented

* Corresponding author.
*E-mail address:* bworonko@uw.edu.pl (B. Woronko).

https://doi.org/10.1016/j.geomorph.2024.109434
Received 13 March 2024; Received in revised form 19 September 2024; Accepted 20 September 2024
Available online 21 September 2024

with respect to ice-flow direction (Sutinen, 1992; Knudsen et al., 2006; Sutinen et al., 2014). They are recorded in various regions of the world and in various morphological situations (Aartolahti, 1974; Lagerbäck, 1988; Johansson and Nenonen, 1989; Eyles et al., 1999; Boone and Eyles, 2001; Calmels et al., 2008; Sutinen et al., 2014; Paulen and McClenaghan, 2015; Alexanderson et al., 2022). They are exemplified as Pulju moraines (Johansson and Nenonen, 1989; Sutinen et al., 2014) and Veiki moraines (Lagerbäck, 1988; Lindqvist, 2020; Alexanderson et al., 2022), or as hummocky stagnant-ice features (Eyles et al., 1999; Knudsen et al., 2006). They form in an irregular pattern of randomly oriented oval depressions (Greenwood et al., 2023). Their origin is associated with debris-covered stagnant ice downwasting into water-filled depressions (e.g. Clayton and Moran, 1974; Lagerbäck, 1988; Johnson et al., 1995; Eyles et al., 1999; Knudsen et al., 2006; Alexanderson et al., 2022), water-saturated diamicton that was forced under pressure upwards into basal crevasses and fractures in the ice-sheet base (Johansson and Nenonen, 1989; Eyles et al., 1999; Boone and Eyles, 2001; Sutinen et al., 2014) or, alternatively, as the subglacial meltwater idea (Munro and Shaw, 1997; Peterson et al., 2017).

This research describes complex ridges and pits in the Żarnowiec Moraine Plateau near Wejherowo in northern Poland (Fig. 1), as identified from digital relief models. The ridge and pit complex we present here is morphologically unique within the areas covered by the last Scandinavian Ice Sheet across the entire Central European Lowland. They are similar in setting to other features in the above- mentioned region, but are distinct in their presentation as a series of ridges of relatively uniform width that are circular, branching, straight or curved, sometimes chain-like—that enclose depressions commonly filled ≤7 m thick with lakes or organic sediments like lake gyttja and peat (Błaszkiewicz and Danel, 2019). Błaszkiewicz and Danel (2019) associated the formation of these forms to the process of permafrost degradation, calling them pingo remnants. Therefore, when setting out to study the morphogenesis of the ridges and pits, we adopted two alternative research hypotheses to account for their genesis, the studied forms are a result of periglacial processes, as a periglacial origin has already been suggested by Błaszkiewicz and Danel (2019), or they arose as a result of processes in a glacial environment. The research objectives are to: 1) show the morphological characteristics of ridges surrounded pits on the Żarnowiec Moraine Plateau; 2) determine their spatial distribution in the region and within the study fields; 3) identify the variability of ridges accompanied the pits; and 4) then discuss the genesis of these features.

## 2. Study area and geological setting

The research area is located on the Żarnowiec Moraine Plateau in central northern Poland and within the range of the last Scandinavian Ice Sheet (SIS; Fig. 1). The morphological pattern of the area was formed

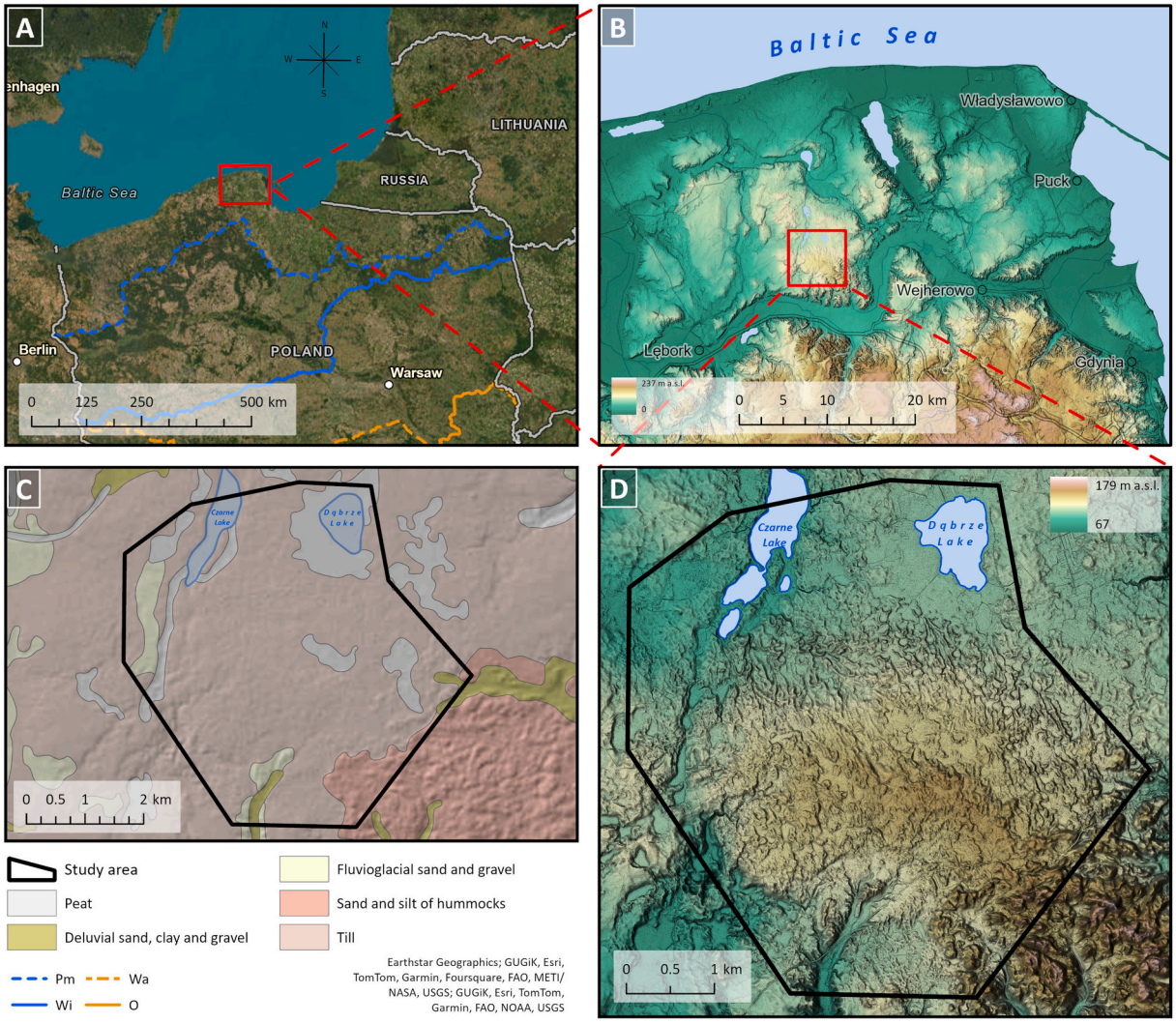


**Fig. 1.** Location of study area against the background of: A. extent of Weichselian Ice Sheet (Wi – LGM, Pm – Pomeranian phase) and Saalian Ice Sheet (O – maximum, Wa – Warta phase); B. large relief features; C. geological setting of study area (Danel and Borecka, 2020, revised); D. high-resolution digital terrain model.

during the ice advance from the north and subsequent ice-marginal recession in the Pomeranian phase, which is dated to 16.8–16.7 ka cal. BP (Rinterknecht et al., 2014; Tylmann et al., 2019, 2022; for a compilation of previous studies see Marks et al., 2023). In the central part of the Żarnowiec Moraine Plateau, there is a roughly east–west-oriented watershed that peaks at 179.14 m a.s.l. (Wysoka Mountain). To the north of this division, the surface of the plateau decreases to 106 m a.s.l. in the vicinity of Lake Dąbrze, and to the south it falls to ~70 m a.s.l. in the vicinity of the Reda–Łeba ice-marginal spillway. The Żarnowiec Moraine Plateau typically has an undulating, hummocky character. Its characteristic geomorphological features are hummocks, irregular kettle-holes, and tunnel valleys with peat plains and finger lakes at their bottoms (Fig. 1).

The Żarnowiec Moraine Plateau has a continuous cover of ≤260 m-thick Quaternary deposits (Zaleszkiewicz, 2005a, 2005b). It is mainly composed of till, glaciofluvial sand and gravel, sand, silt and clay, accumulated during successive Pleistocene glaciations (Elsterian, Saalian, and Weichselian). The surface of the study area has an almost continuous cover of Weichselian till (Fig. 1C) of thickness varying from a few metres to >20 m. In a few places, that till is overlain by thick sediments that in formation build ice-walled-lake plains. Within land depressions (including tunnel valleys, larger kettle holes, and ramparted depressions), there are often organic sediments like peat and lake gyttja.

The area of detailed study is part of a moraine plateau covering ~25 km$^2$, which stretches to the west between the tunnel valley containing Lake Czarne, to the east to a region of hummock hills, and to the north to Lake Dąbrze (Fig. 1C).

## 3. Methods

To show the morphological diversity of the ridges and pits in the study area, 14 test fields were selected, each measuring 0.5 km × 0.5 km (the area of each field being 0.25 km$^2$). The test fields were selected to: 1) represent the diversity of ridges and pits in the study area; 2) include relatively uniformly developed ridges and pits; and 3) locate different altitudes and aspects within the plateau—i.e., on a slope with

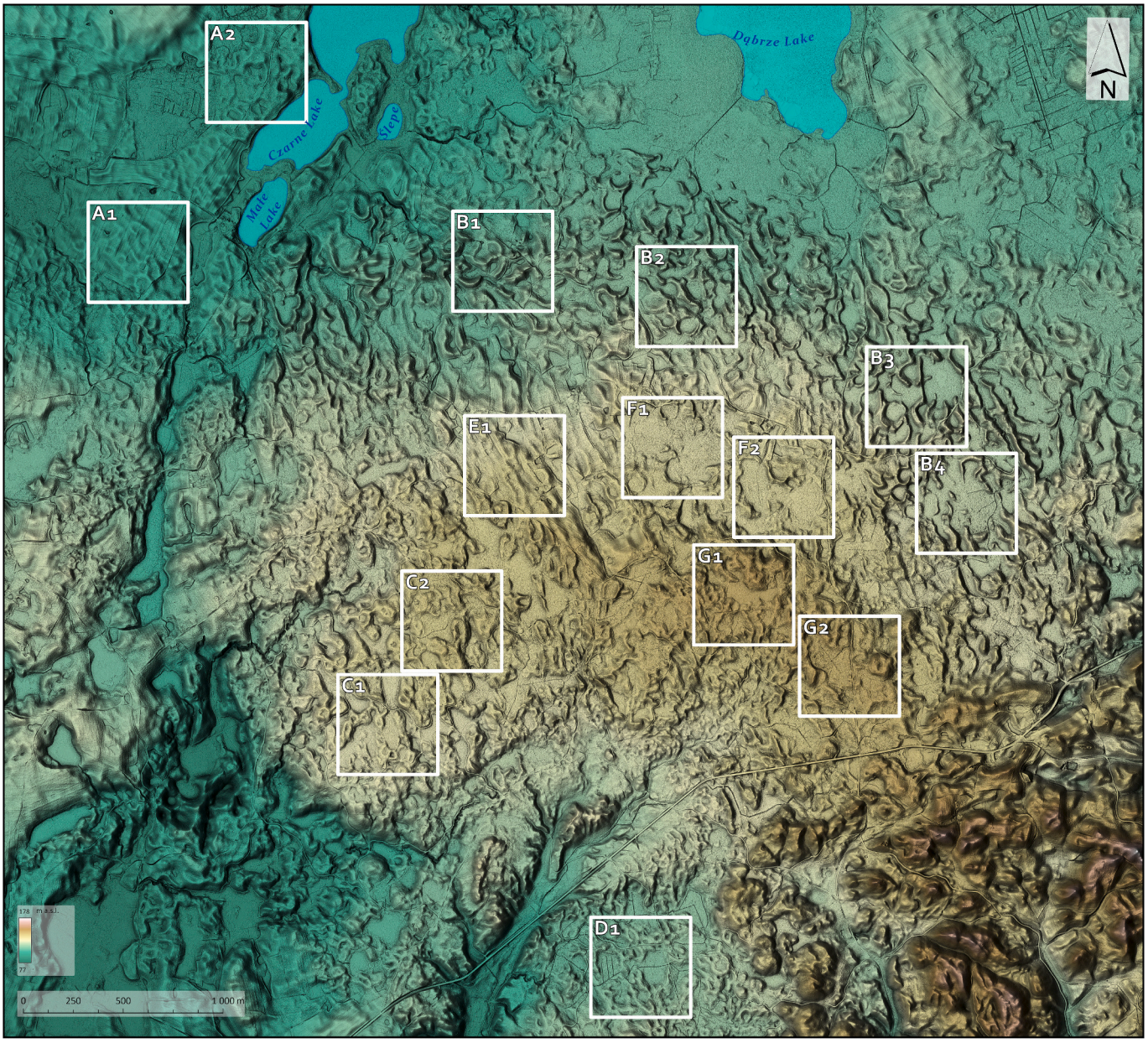


**Fig. 2.** General view of location of ridges and pits in study area showing test-field locations (A1, A2, B1–B4, C1, C2, D1, E1, F1, F2, G1, and G2).

northern–southern exposure and on the top of plateau. Test fields were designated on a plateau near the tunnel valley with Lake Czarne (A1–A2), on a north-facing slope of the plateau (B1–B4 and E1), on the watershed (F1, F2 and G1–G2), and on a south-facing surface of the plateau (C1, C2, and D1; Fig. 2).

In order to conduct a detailed analysis of the terrain morphology, high-resolution (1 m × 1 m) lidar, laser scanning data were processed with 1-m horizontal resolution and average elevation error of 0.2 m. All spatial analyses were performed using ArcPRO software, including: 1) DTM visualizations; 2) form vectorization; 3) analyses of the morphometric parameters of ridges and pits; 4) statistical analysis; and 5) a summary of results. Additionally, scripts available in the Whitebox Geospatial Analysis Tools package were used (Lindsay, 2016).

The ridges and pits were analysed in several stages (I–IV).

In stage I, multidirectional hillshade relief models with varying degrees of elevation (from 1 to 5) were generated. These images combine visualizations of form lighting from six different directions. This made it possible to visualize the relief shading, eliminating problems between overexposed and shadowed areas of the map (Smith and Clark, 2005; Nagi, 2014; Kokalj and Hesse, 2017, Chandler et al., 2018). In stage II, rasters were generated using the *openness* parameter (Yokoyama et al., 2002), which together with the *slope* and *hillshade* layers and using appropriate combinations of symbolization parameters, enhanced the readability and sensitivity of the Red Relief Image Maps (RRIM) relief model (Chiba et al., 2008; Kokalj and Hesse, 2017; Daxer, 2020). In stage III, the geomorphons algorithm was used on the processed DEM model (Jasiewicz and Stepinski, 2013; Dąbrowski and Jasiewicz, 2014). The obtained geomorphon images facilitated the identification of morphological features during their vectorization stage. Stage IV consisted of compiling the terrain visualizations—i.e., DEM, RRIM, and geomorphons. Analysis of the geomorphons allowed us to distinguish ten topographical forms in the studied area, the main features being slopes, then spurs, followed by valleys, hollows, ridges, footslopes, flat areas, peaks, pits and shoulders.

The most characteristic relief features here directly relate to two morphological features: 1) positive—ridges; and 2) negative—central depressions that we refer to as 'pits' (Fig. 3). Each of the two form parts were analysed separately. The ridge courses have been manually mapped as lines coinciding with their axes (Fig. 3). The pit shapes were drawn using surface objects (polygons). For large pits, boundaries were taken to be ridge fragments protruding sometimes only 0.2 m above the level of a pit's peat infill. Within the designated study fields, 1898 ridges and 802 pits were analysed.

In work-stage V, morphometric parameters were calculated for the vectorized objects. For negative forms (pits), the *Minimum Geometry Bounding* tool and the *Convex hull* function were used (Jorge and Brennand, 2017), the following parameters were calculated: 1) the major axis (orientation) of the pits (oval; L); 2) the shortest axis of the pits ($W_d$); 3) azimuth of major axis ($D_L$) for each polygon; and 4) the absolute height of the pit's centre point ($C_p$; Fig. 3). Basin area (A) was calculated from the outline of the basin's infill. The resultant data was used to calculate the basin-elongation index using the formula:

$$(E = L/W_d) \quad (1)$$

The E parameter always takes a value >1. The closer the value is to 1, the more isometric the object is, i.e. the longer axis (L) is close to or equal to the shorter axis ($W_d$).

To obtain the ridge-morphometric parameter, profiles perpendicular to the ridge were determined, from the axis of the ridge to its foot (≥95 profiles for each research field – A1–A2, B1–B4, C1–C2, D1, E1, F1, and G1–G2), on which 3D Analyst tools were then used. Average parameters were obtained for selected sections of the profile for relative height of ridges (H) and average slope inclination ($a_s$). Parameter H was calculated as the highest point in a shape profile, and was drawn perpendicular to a ridge course. The shape's height was measured at several points, taking into account the ridge-height differences within one form. Ridge width ($W_r$) was determined by border measurements of the two closest neighbouring pits (Fig. 3).

The density index of ridges per 1 km$^2$ ($D_R$) was calculated for all 14 test fields, according to the formula:

$$D_R = L_r/A_f \quad (2)$$

where $L_r$ is the sum of ridge lengths (km) in a given test field, and $A_f$ is the surface area of the test field (km$^2$).

Similarly, the density of pit per 1 km$^2$ ($D_D$) was calculated as:

$$D_D = nD/A_f \quad (3)$$

where $n_D$ - is the total number of pits in a test field, and $A_f$ - is the surface area of test field (km$^2$).

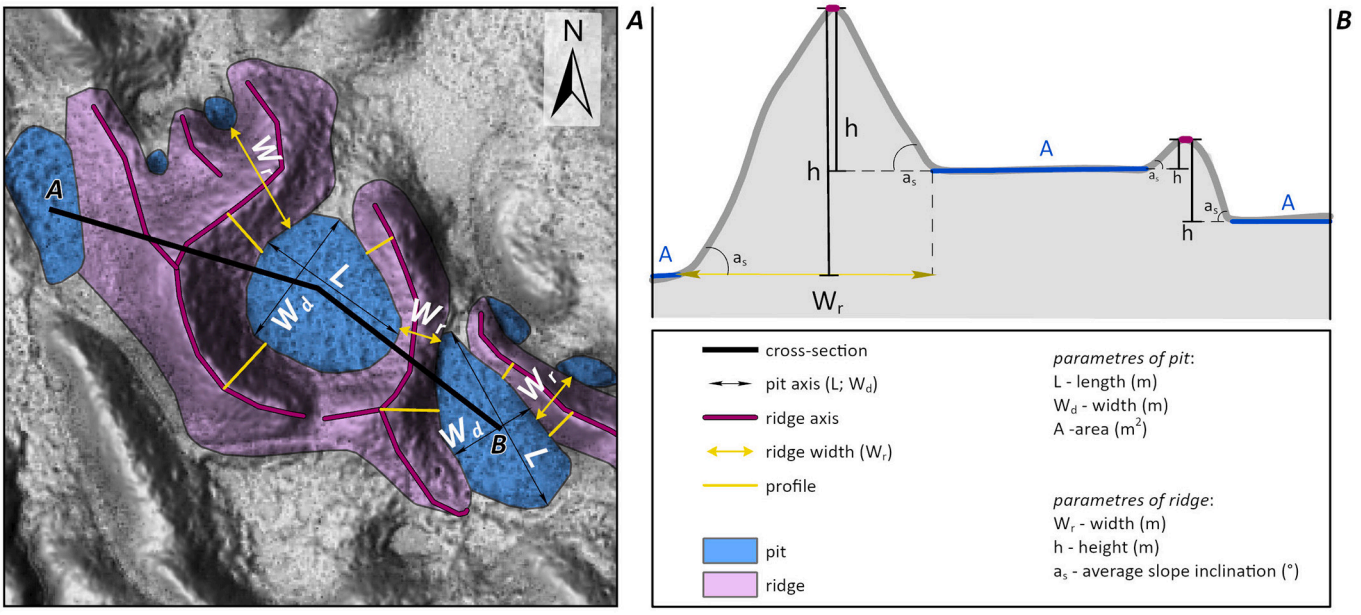


**Fig. 3.** Morphological elements of tested ridges and pits and their measured parameters.

Further, the percentage of the area occupied by pits was calculated for each research field. Thus, a ridge–pit relationship was distinguished in the studied area as based on the obtained results and qualitative comparison through zones of similarly.

## 4. Results

In total, 801 pits and 1898 ridges were measured. They were divided among the 14 test fields (A1, A2, B1–B4, C1, C2, D1, E1, F1, F2, G1, and G2) that represent the diversity of ridges and pits in the study area (Fig. 4). The forms differ in area (A), length of long (L), and short axes ($W_d$), and the ridges' widths ($W_r$), heights (H), and slope inclinations ($a_s$) (Figs. 3–14).

### 4.1. Positive forms

#### 4.1.1. Relief of ridges

The characteristic features of ridges in the studied area are as follows:

- The ridges are an integral part of the pits in that they are separate from one another, and do not occur in isolation but connect to neighbouring ridges in a branching or chain-like fashion (Figs. 5, 6).
- All test fields are dominated by single ridges that are predominantly curved, with a sharp ridge, a uniform width and profile, and steep slopes (Fig. 6A, C).
- In test fields C1, C2, and D1, which are located on the southern slope of the moraine plateau (Fig. 2), the ridges are wider than in the test fields B1–B4, and have clearly marked flat tops surrounding large pits. A top such features are small round pits with diameters of just a few tens of metres (Fig. 6D, E).
- Double-peaked ridges are recorded, resulting from ridges having merged with those of adjacent pits. In this case the pit between two ridges is not filled with peat (Fig. 6B).
- There are ridges that run parallel to each other, echoing their shapes in close proximity to each other (Figs. 5, 6C). These are ridges whose radius of curvature is in precisely the opposite direction (Fig. 6B).
- There are ridges that are not of uniform height along the entire length of the ridge, ridges that surround a single pit. Sometimes these

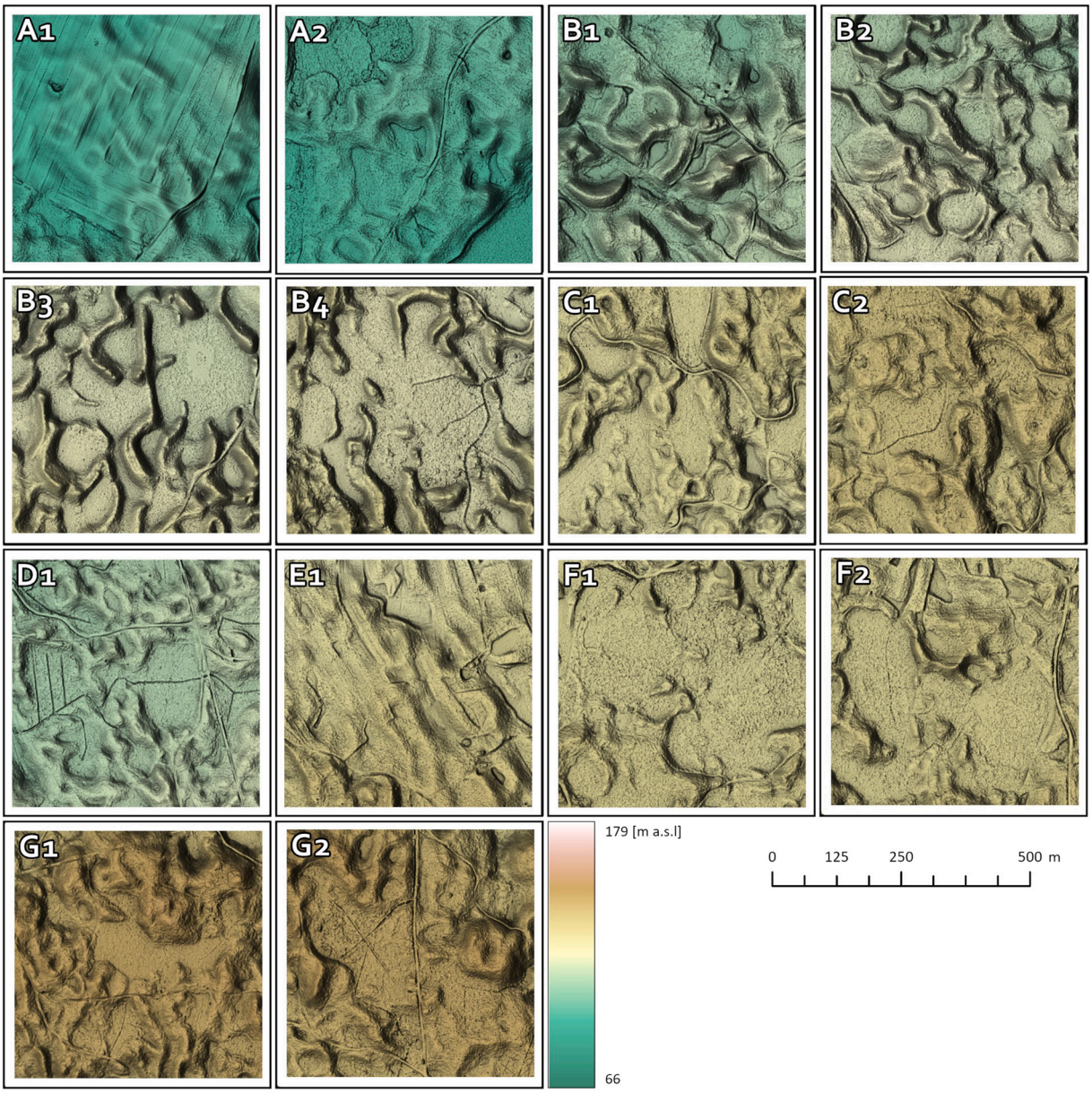


**Fig. 4.** Diversity of relief of ridges and pits within designated test fields (A1, A2, B1–B4, C1, C2, D1, E1, F1, F2, G1, and G2). For test-field locations, see Fig. 2.

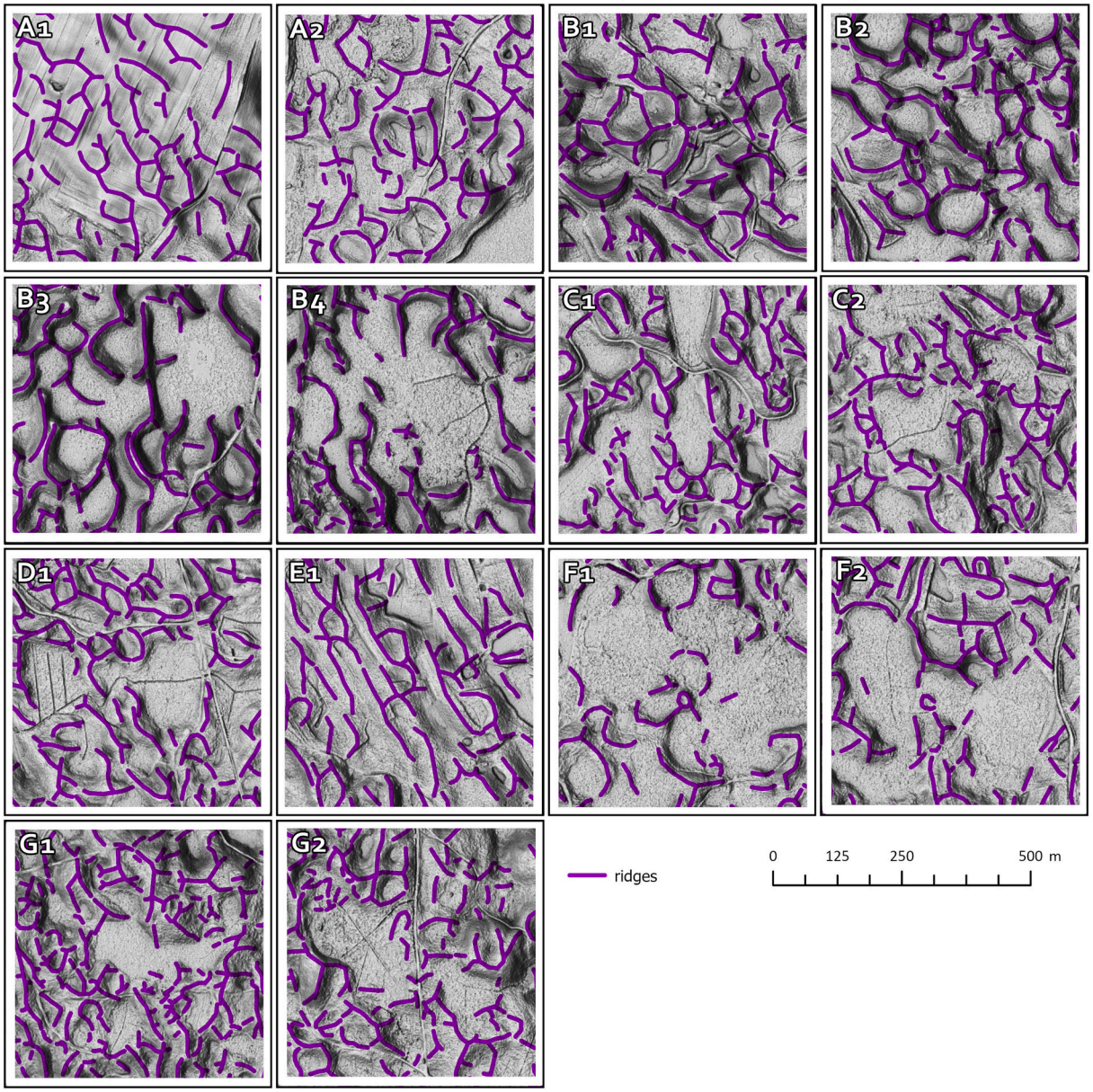


**Fig. 5.** Course of ridges surrounding pits in individual test fields. For test-field locations, see Fig. 2.

are linked to each other in a step-wise fashion or disappear below the peat level (Fig. 6D).

- Ridges surrounding pits commonly have a single or several similar erosional score of small width and depth connecting adjacent pits, possibly providing water drainage (Fig. 6B). Such forms may occur at any ridge separating individual pits that are part of a step-wise configuration. Some ridges have an amphitheatre shape, with high walls on three sides and another open to the adjacent pit. Only a few forms are enclosed by an unbroken ridge (e.g. as in fields B1–B4; Figs. 5, 6D, E).
- It is common for the ridges to form closed-ring forms, but not ridges are like this. Elongated and parallel ridges occur, often with a slightly wavy course (Fig. 6B, D, E), between which elongated pits occurs in the form of a pit-accommodating valley that contains a pit but is not currently used by flowing water (Fig. 6G).
- Ridge slopes present no signs of slope erosions (rills, gullies).
- Some ridges are partly buried under peat cover (Błaszkiewicz and Danel, 2019). Only the top of the ridge protrudes from under this cover, attaining a height of only 0.15–0.20 m, or, on occasion, more (Fig. 6H).

#### 4.1.2. Statistical analysis

The height of the ridges ranges from 0.2 to 9.2 m with most between 0.7 and 2.6 m. The height of 90 % of the ridges does not exceed 4 m (Fig. 7A; Table 1). The highest ridges were recorded in the G1 test field in the east of the moraine plateau (Fig. 2). However, such high ridges occur only occasionally. Test fields B1–B4 stand out clearly for the height of their ridges, which is much higher than that of the other test fields (Fig. 7A). All these test fields are located at the base of the northern moraine plateau slope (Fig. 2). The lowest ridges were measured in A1 and A2 (Fig. 7A).

The width of the ridges ranges from 3.2 m to (in individual cases) 110 m, with most between 20 and 40 m. The ridges in test fields A1 (30–40 m) and G1 (20–30 m) have the most uniform ridge widths. This parameter is most diversified in test fields B1 (27–56 m; Fig. 7C; Table 1).

The slope inclination of ridges also varies both between fields and

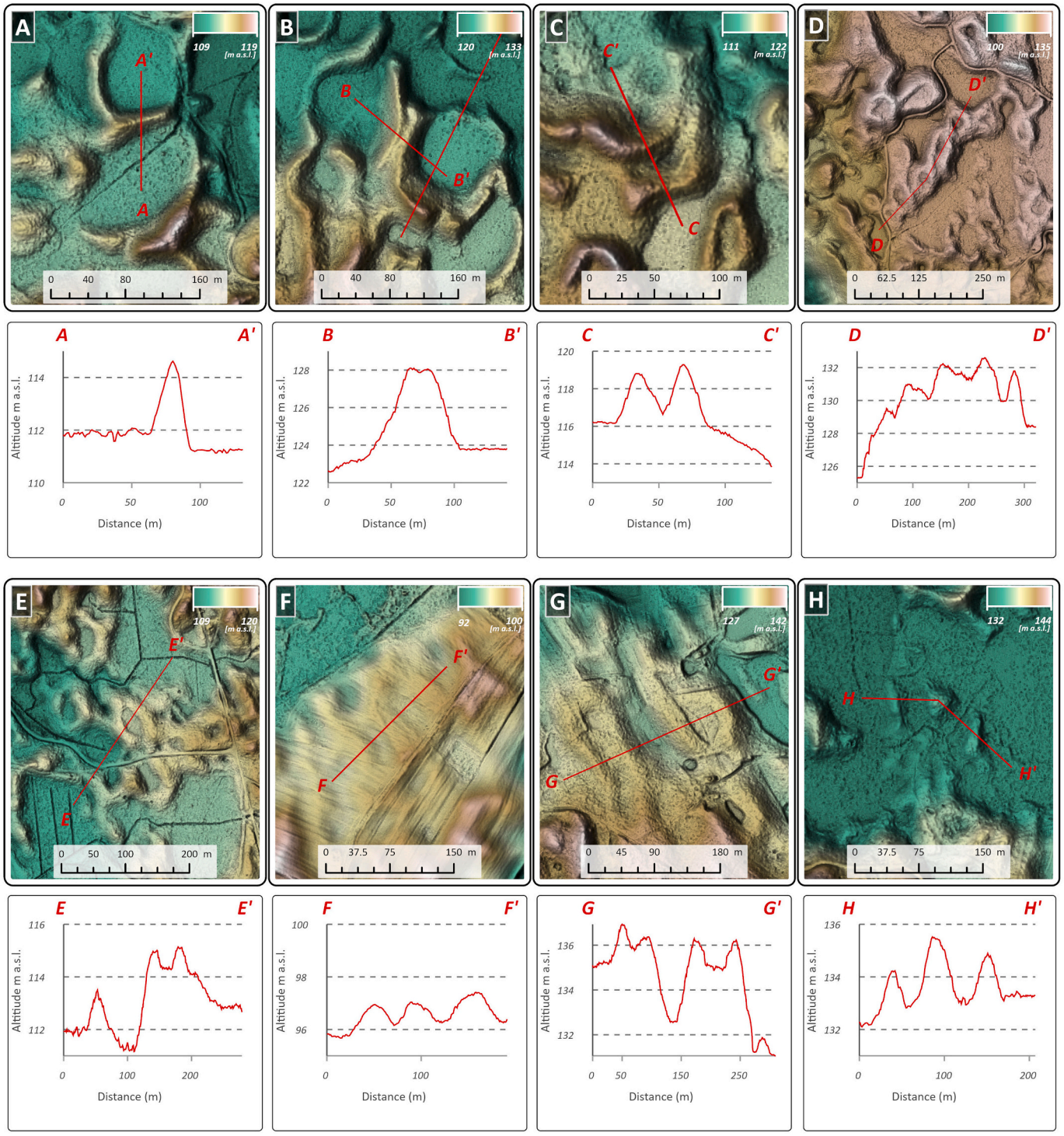


**Fig. 6.** Diversity of ridge forms surrounding pits: A. single ridge with cross-section A–A′, varied height of ridges surrounding single pit; B. double ridge and cross-section B–B′, C. two parallel ridges towards each other with cross-section C–C′; D. width ridge with a series of small pits with cross-section along the ridge D–D′; E. width ridge with a series of small pits with cross-section parallel the ridge E–E′; F. wide and low height ridges surrounding small diameter and size with cross-section F–F′; G. elongated and parallel ridges with cross-section G–G′; H. ridges are partly buried under peat cover with cross-section H–H′.

within individual fields (Figs. 7B, 8A). The average slope inclination is 6°, while the maximum slope is 19–20°. Test fields B1–B4 are characterized by the steepest slope, with an average above 7.5°. Field B3 stands out clearly against this background, with an average slope inclination of the ridges of 9.6°. However, test fields A1 and A2 have the shallowest inclination of ridge slopes. The average values for these fields are 3.5° and 4°, respectively (Fig. 8A; Table 1). In these test fields, this angle is also the most uniform of all forms.

The differences between individual test fields are shown by the $D_R$ parameter—i.e. ridges density given as km/km$^2$. It varies from 12.4 km/km$^2$ in F1 to 21.3 km/km$^2$ in D1. Similarly high values were recorded in test fields B2 (21.2 km/km$^2$) and E1 (21.1 km/km$^2$). There is also a correlation between the height of ridges and their slope inclination. The higher high the ridges, the greater its slop inclination (Fig. 8A; Table 2).

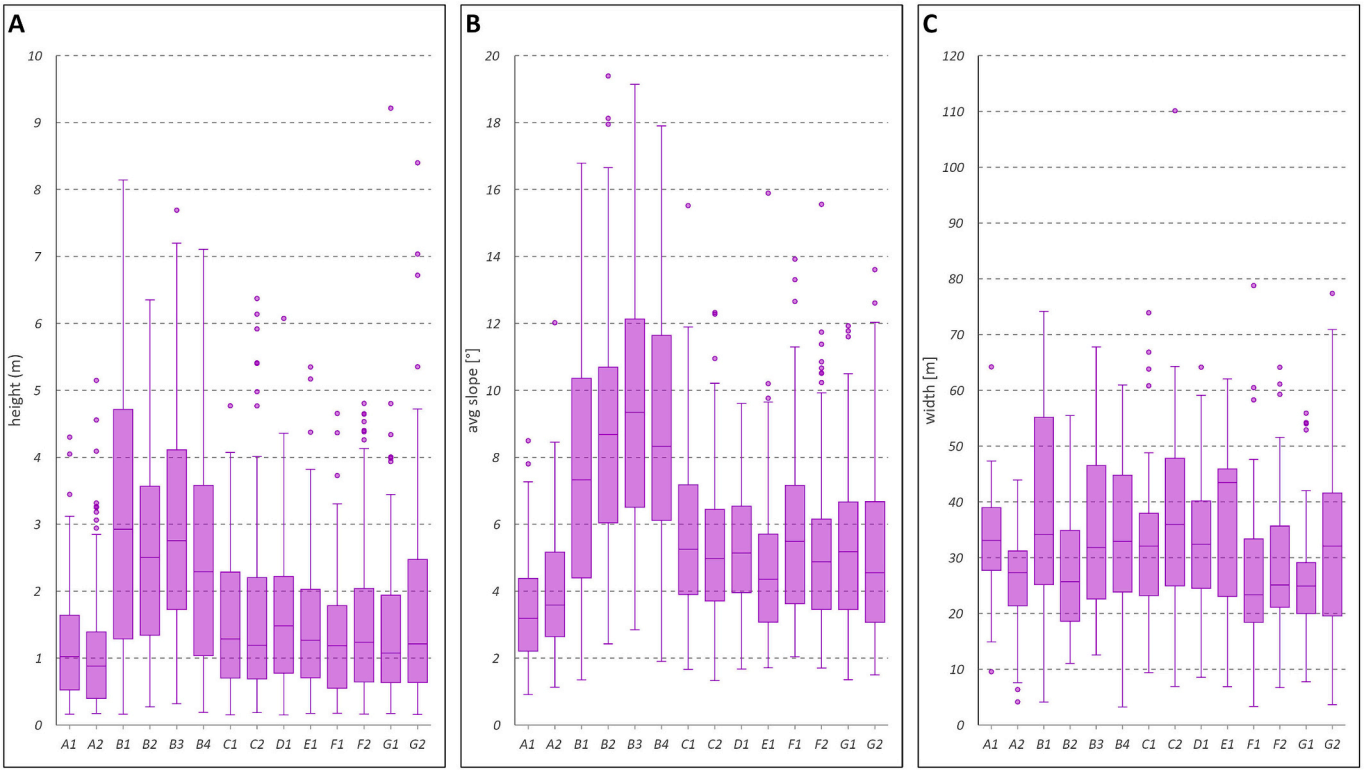


**Fig. 7.** Box-plot graphs of ridge-parameter variability within test fields ($n$ = 1487): A. ridge heights; B. ridge-slope inclinations; C. ridge widths.

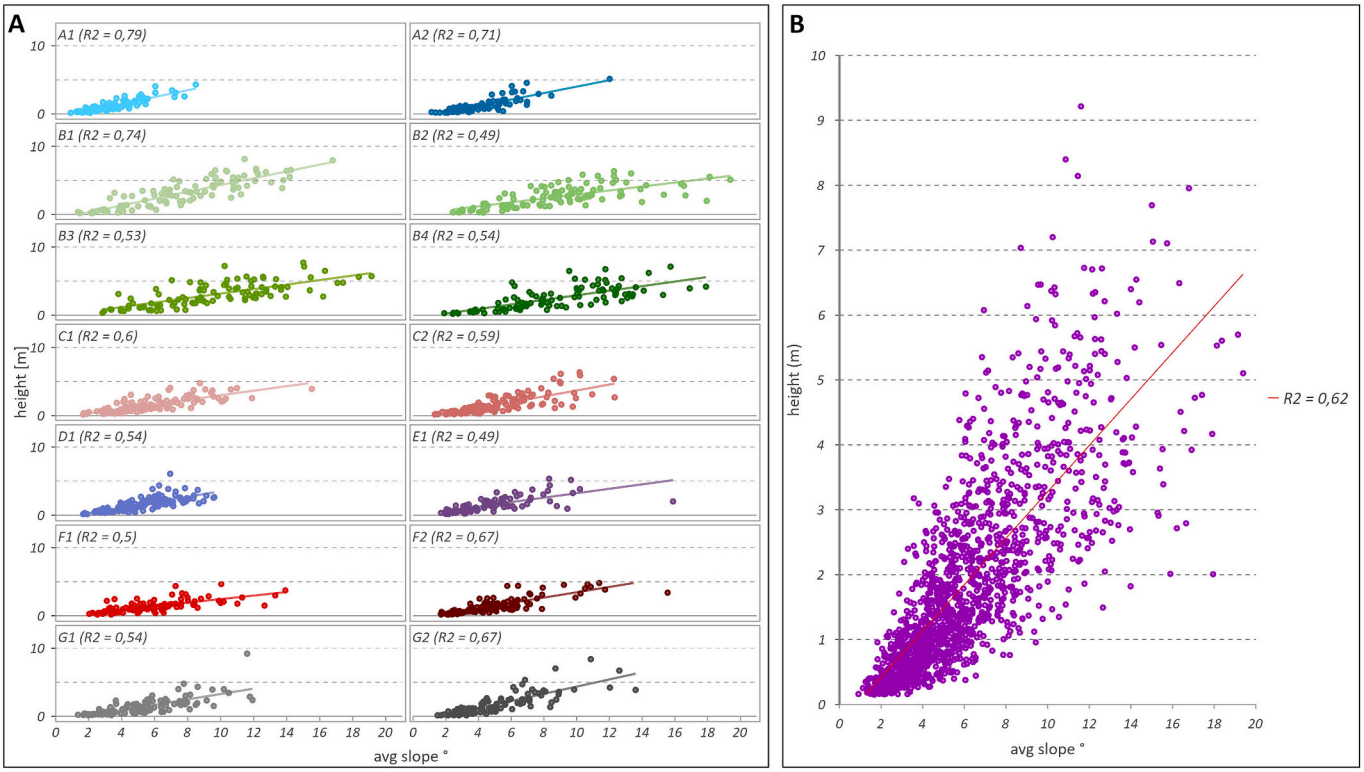


**Fig. 8.** Parameters of the ridge inclinations of tested forms (n = 1487): A. variable ridge inclination within test-fields; B. relationship between height of ridges and their slope.

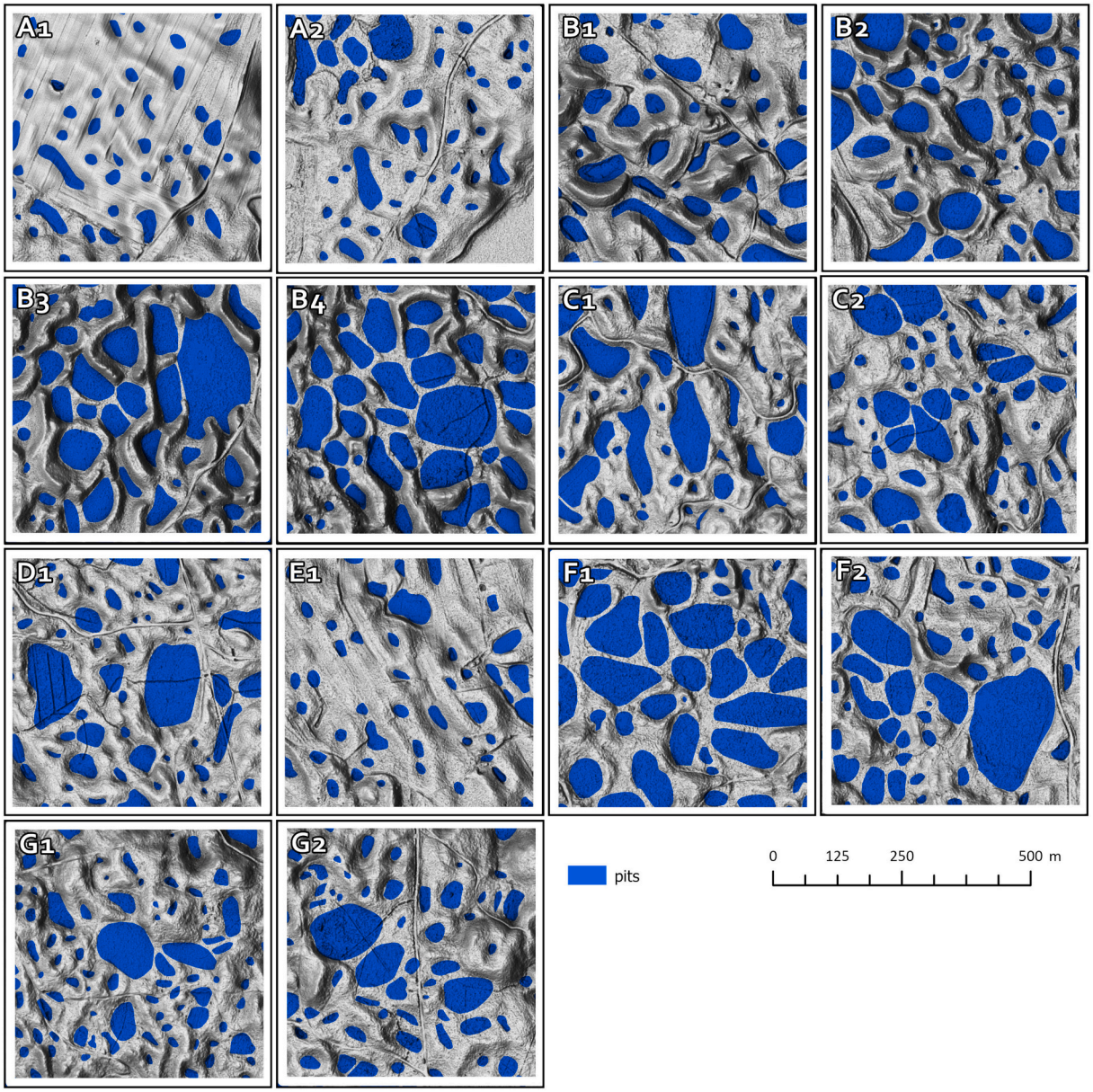


**Fig. 9.** Characteristic features of study area pit relief: A. pits linked to each other in a step-wise fashion with cross-section A–A′; B. amphitheatre arrangement of ridge surrounding pit with cross-section B–B′; C. fragments of ridges protruding above peat filling pit with cross-section C–C′.

### 4.2. *Negative forms*

#### 4.2.1. *Relief of pits*

The pits on the Żarnowiec Moraine plateau have the following characteristics:

- The pits occur in a network of many pits and are approximately (and to varying degrees) circular in shape. Some are irregular in shape (Figs. 9, 10).
- Pits are linked to each other in a step-wise fashion, with several pits one above the other. They are separated from each other by a ridge that is low on the side of the upper pit, while steep and relatively high on the side of the lower pit (Fig. 10A). Groundwater levels in adjacent pits are perched at different heights, which suggests a low permeability of the ridge-building sediments.
- Pits are separated by a uniform ridge rather than a wider divide (Figs. 9, 10).
- Some pits are surrounded by high, steeply sloping ridges on three sides and open on one side to an adjacent pit. In such cases, the gap in the ridge is wide with a similar height to its adjacent pit (Fig. 10B).
- Some of the test fields (F1, F2, B4) contain pits with an exceptionally large area and irregular shape that are referred to as compound pits (Figs. 9, 10C). Often, the outlines of apparently buried ridges are visible on their surface, slightly protruding above the level of organic sediments (Fig. 10C).
- A vast majority of pit bottoms have a flat surface characterized by slight elevations associated with the presence of raised peat bogs (Fig. 10A). In the case of compound pits there are the outlines of buried ridges. In the case of small pits, high deviations of surface levels are not recorded.
- A vast majority of pits are filled with organic sediments—i.e. lake gyttja and peat (Błaszkiewicz and Danel, 2019).

#### 4.2.2. *Statistical analysis*

Pit-relief feature analysis results from the Żarnowiec Moraine

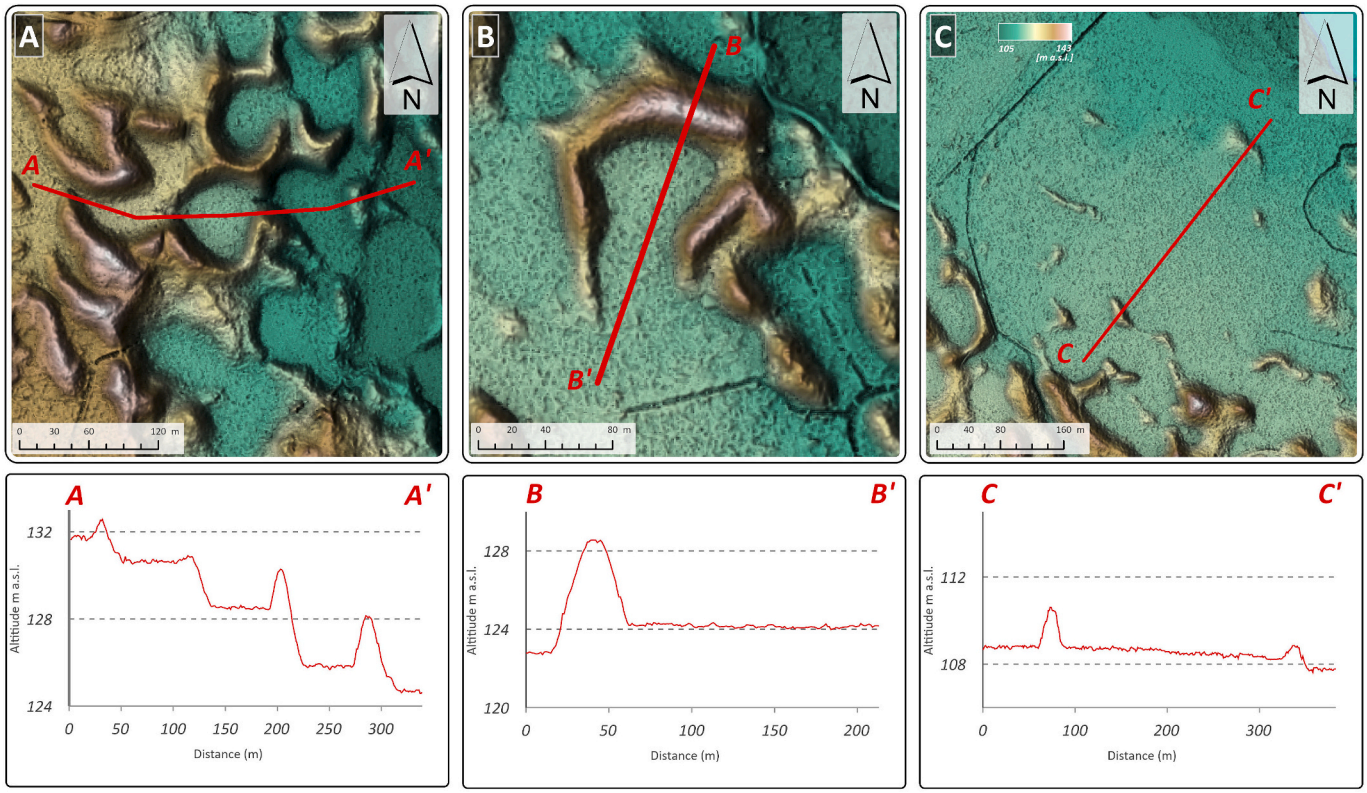


**Fig. 10.** Pit-size diversity within test fields. For test-field locations, see Fig. 2.

Plateau area demonstrates that the number of pits in individual research fields varies from 42 in field F1, through 55 in C2, to 62 and 66 in fields F2 and G2. The G1 test field clearly stands out against this background as to the pits in this field (Figs. 9, 11; Table 3). 87 % of them have an area up to 3000 $m^2$. However, pits with an area of up to 500 $m^2$ clearly dominate among them (Fig. 12A). Compound pits (outliers) occur in the F2 test field (28,108 $m^2$), the B3 field (23,827 $m^2$), and the B4 field (16,384 $m^2$) (Fig. 12A; Table 3). The first field is located in the upper part of a northern-facing slope of the plateau and the other two reside at its base (Fig. 2). Additionally, these same three text fields (B3, B4, and F2) have the greatest pit variation in terms of surface size—i.e. next to very large compound pits, there are small and very small (<200 $m^2$) ones (Figs. 11, 12). The smallest pit-surface areas are found in fields A1, E1, and G1, which are also characterized by the smallest differences in sizes (Figs. 9, 11, 12). They are located on the plateau extending west of Lake Czarne, in the upper part of northern-facing slopes, and upon the moraine plateau (Fig. 2). The average pit sizes in these fields are 585 $m^2$, 686 $m^2$, and 639 $m^2$, respectively. Pit shapes show that roughly oval pits decidedly dominate, regardless of their size (Figs. 9, 13C), in which the longer axis (L) ranges from 30 to 70 m. These constitute ~80 % of all pits. There are also those in which the L value exceeds 200 m, although their share is only 0.4 % of all pits; they were recorded in test fields B3 and F1 (Fig. 13C). A characteristic feature of the examined test fields is the high variability of L-parameter values. The differences were greatest in test fields B1–B4 and F1 and smallest in fields A1–A2, E1, and G1 (Fig. 13C; Table 2).

The value of the short axis ($W_d$) is in the range of 20–30 m for most pits. These constitute 47 % (Fig. 8C). Similar to the L index, the length $W_d$ of the pit axis was most variable in test fields F1, B2, and B3. Conversely, test fields A1, E1, and G1 vary the least in terms of this parameter (Figs. 12C, 13B; Table 3).

The elongation ration (E) varies from 1 to 2, although values vary within individual test fields; some individual pits reach 3–4, which is indicative of extreme elongation. The average elongation ratios for test field range from 1.62 to 1.89. The highest average E values are recorded in test fields B1, C1, and F1, and the lowest values occurred in test fields A1 and A2 (Fig. 13C; Table 2). There are very few basins that do not show elongation (Fig. 9). Near-isometric pits are primarily a characteristic of extreme size—i.e. are very large or very small (Fig. 13C).

The highest $D_D$ values are found for the G1 and D1 test fields, at 348 pits and 276 per $km^2$, respectively. By contrast, the lowest values were recorded in fields F1 (168 per $km^2$) and E1 (184 per $km^2$). $D_D$-index values are also low in fields A1 (192 per $km^2$) and A2 (196 per $km^2$). However, in test fields B1–B4, this value ranges from 204 to 228 pits per $km^2$ (Table 2).

Pit-longitudinal axis (L) orientation for all test fields show slight variations in pit orientation, although all areas show a preferred orientation. A prominent mode occurs in nearly all test areas between 310 and 340. However, other prominent modes also occur, including 10–30, 70–80, and 250–260 (Fig. 14).

Considering all the measured parameters of the pits themselves, as well as the ridges, five zones (I—V) are identified (Fig. 15). Each zone differs in pit and ridge morphology (Figs, 2, 5, 7–11, Table 3). The test fields also differ in their a.s.l. position (Fig. 16).

## 5. Discussion

### 5.1. The origin of ridges and pits: analogous periglacial and glacial forms

The relief of the research area clearly differs from neighbouring regions. The study area's characteristic feature is the cluster of ridges and pits we describe here, which borders the vast kettle-hole-accommodating Lake Dąbrze to the north, the tunnel-valley-accommodating Lakes Czarne and Żurawieckie to the east, the Reda–Łeba ice-marginal valley to the south, and a field of hummocks that clearly tower above their surroundings to the east. In this discussion, the ridges and pits in the study area will be referred to as the ZMP ridges and pits, named after the Żarnowiec moraine plateau (Fig. 2).

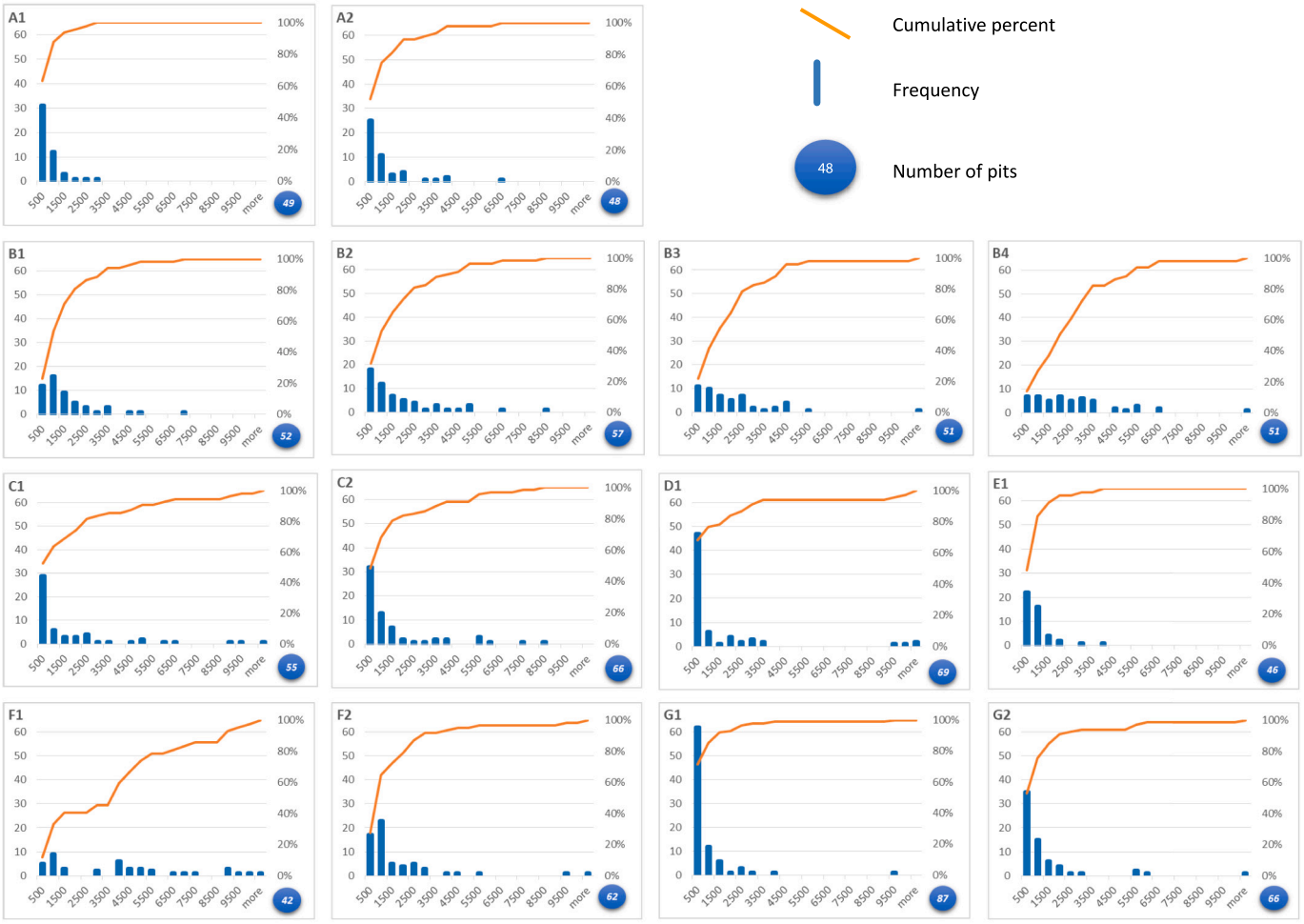


**Fig. 11.** Diversity of size of pit area in test fields and number of pits in each (blue circle in lower right corner).

During the last glaciation, while the ice sheet was at its maximum range, the studied area was in the marginal zone of the ice sheet (Rinterknecht et al., 2014; Tylmann et al., 2019, 2022); it was the Weichselian Ice Sheet glaciation that shaped the relief of this area (Zaleszkiewicz, 2005a, 2005b). During the recession of this ice sheet, permafrost aggraded on the surface of the freshly exposed glacial landscape (Kozarski, 1986, 1991; Słowiński et al., 2015; Petera-Zganiacz and Dzieduszyńska, 2017; Woronko and Dąbski, 2023). This permafrost may have merged with relict permafrost originating from the advance phase of the ice sheet (Błaszkiewicz, 2011; Van Loon et al., 2012). Permafrost may have survived through the Bølling–Allerød warming in the study area, and its partial aggradation most likely occurred during the Younger Dryas cooling (Petera-Zganiacz and Dzieduszyńska, 2017; Dzieduszyńska and Petera-Zganiacz, 2018). It was only with the beginning of the Holocene, at the turn of the Preboreal and Boreal periods, that the final degradation of permafrost occurred in northern Poland (Błaszkiewicz, 2011; Van Loon et al., 2012; Błaszkiewicz et al., 2015; Słowiński et al., 2015). Therefore, when setting out to study the morphogenesis of these ridges and pits, we adopted two alternative research hypotheses for verification. The first one was that the studied forms are the result of periglacial processes, and in opposition the second one is that they arose as a result of glacial processes.

### 5.1.1. *Periglacial origin of ridges and pits*

Landforms with ridges and pits similar to those occurring in the study area have been attributed to periglacial processes; some of them have been called "ramparted depressions" (Pissart, 2002, 2003; Demoulin et al., 2018; Ross et al., 2019). In the modern periglacial environment, ridges and pits are either small in form (a few metres across) or large in form (sometimes exceeding 100 m across) (e.g. Wolfe et al., 2014; French, 2017). An example of the first are sorted circles. However, these forms are much smaller than the ZMP ridges and pits, having a typical very high spatial density but have a typical diameter of only 2–3 m and a typical height of only 0.25 m (Hallet, 2013). The second forms are frost mounds, such as collapsed pingos (Watson, 1975) or collapsed lithalsa (French and Dimitroff, 2001; Pissart, 2002, 2003, 2013; Calmels et al., 2008; Demoulin et al., 2018; Ross et al., 2019), which are generally characterized by morphometric parameters similar to the ZMP landforms (Figs. 7–8, 11–13). On the contrary, collapsed pingos have a similar shape and size in terms of the diameter and ridge height, which is why Błaszkiewicz and Danel (2019) suggested linking the genesis of the study-area ridges and pits with the collapsed pingos, which they were referred to as doughnut-like "ring forms". Only a small area comprised of individual forms were analysed by Błaszkiewicz and Danel (2019). However, we consider a collapsed pingo origin for the ZMP ridges and pits to be very unlikely. Within the modern range of continuous permafrost, pingos—despite having sizes similar to the study-area forms—occur as single entities and their spatial density is usually low. Jones et al. (2012) mapped 1247 pingo in an area of ~40,000 km$^2$ in the western Arctic Coastal Plain of northern Alaska. This means that their density is only 0.031 per km$^2$. Grosse and Jones (2011) state that the highest densities of pingos in Asia occur in the central Yakutian Lowland near Yakutsk (28 pingos per 100 km$^2$) and in the Anadyr River Valley (28 pingos per 100 km$^2$). For comparison, in the Mackenzie Delta region,

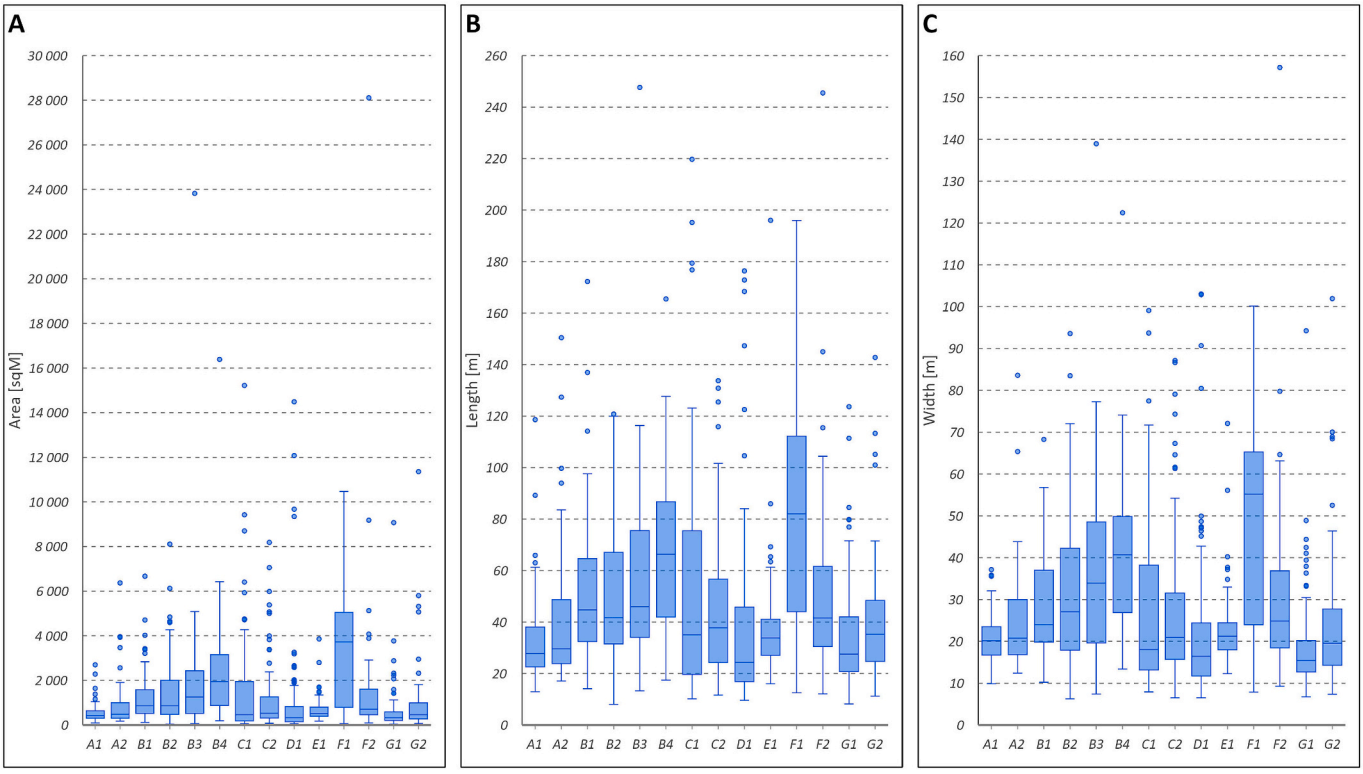


**Fig. 12.** Box-and-whisker graphs: A. size of pit area (A); B. long axis of pit (L); C. short axis of pit ($W_d$).

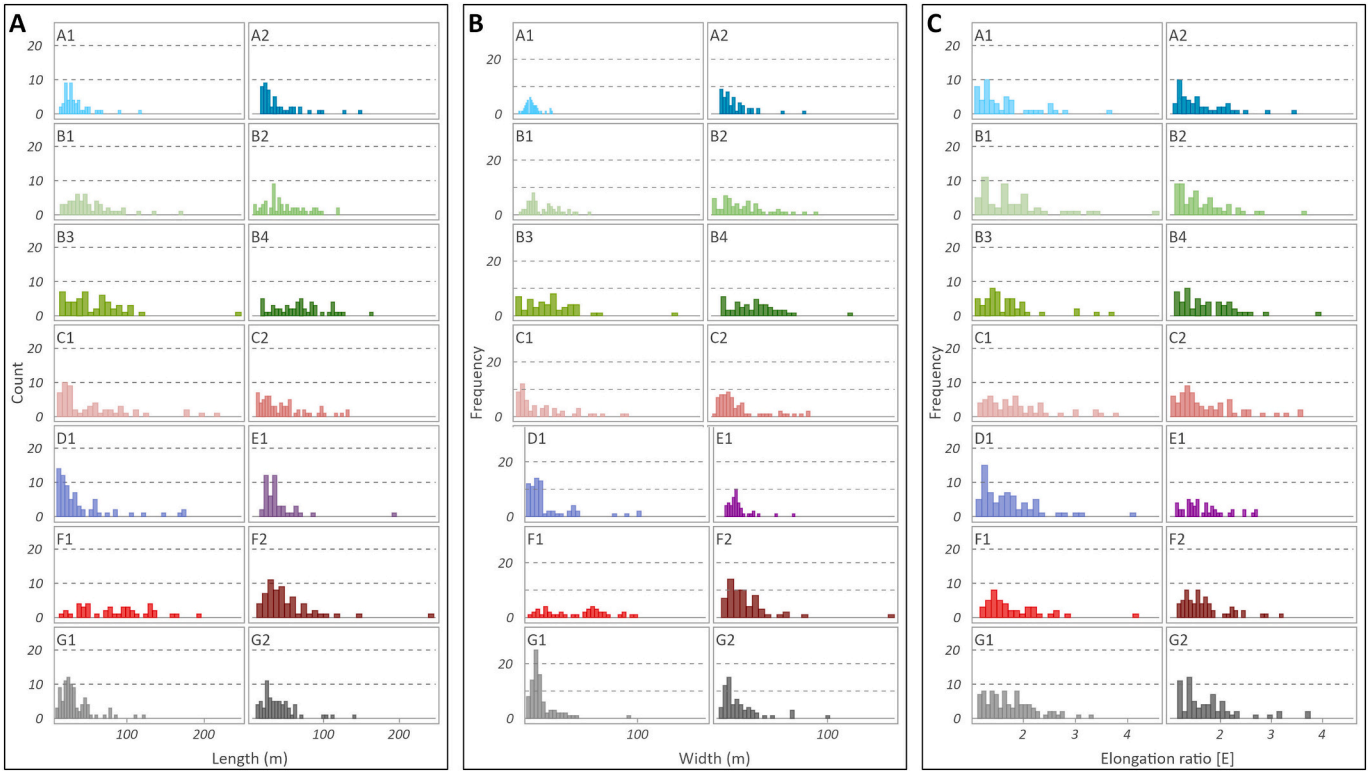


**Fig. 13.** Pit-parameter diversity within test-fields: A. length of long axis (L) pits; B. widths of pits ($W_d$); C. elongation index (E).

their density is only <8 per km$^2$ (Stager, 1956). Wolfe et al. (2021) used a High-Resolution Digital Elevation Model (HRDEM) to analyse pingos on the western Canadian Arctic (WCA) coastal plain and showed that their density is ~0.15 km$^2$. For comparison, the density of the studied ZMP ridges and pits in the Żarnowiec plateau ranges from 168 to as much as 348 per km$^2$ (Fig. 10; Table 2) and is very much higher than what would expect from a pingo form density. Therefor based on these comparisons, we consider it unlikely that the ZMP ridges and pits in the

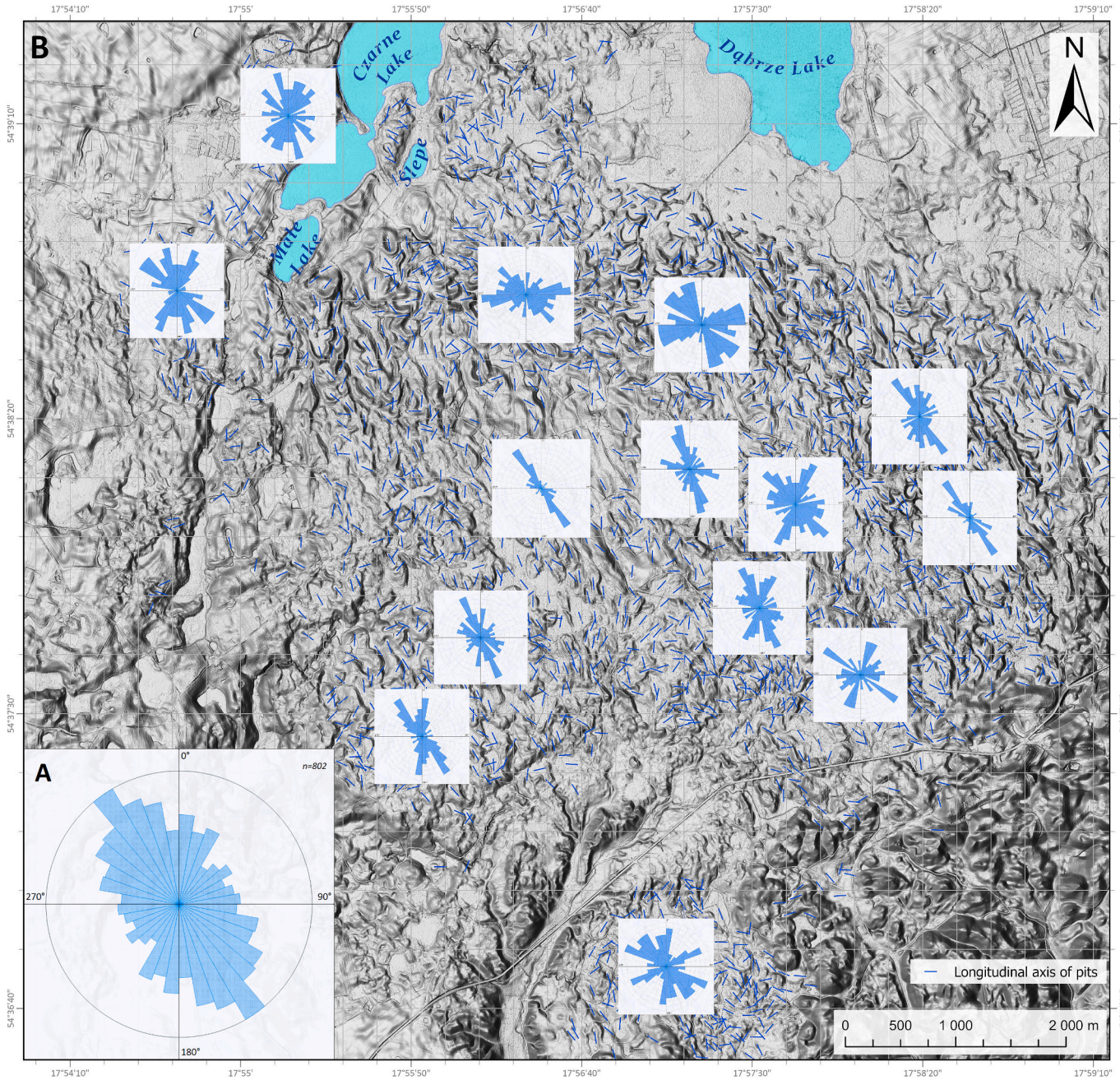


**Fig. 14.** Rose diagrams illustrate orientation of longitudinal axis of pits (L): A. for all pits ($n$ = 802); B. within tested fields.

**Table 1**
Ridge and pit statistics.

| | Minimum | 1st quartile | Median | Mean | 3rd quartile | Maximum |
|---|---|---|---|---|---|---|
| Height (m) | 0.15 | 0.72 | 1.43 | 1.85 | 2.57 | 9.21 |
| Avg slope ° | 0.91 | 3.58 | 5.30 | 6.02 | 7.80 | 19.39 |
| Ridge width (m) | 3,24 | 21.76 | 29.76 | 32.10 | 41,35 | 110.11 |

study area are collapsed pingos.

Another form that should be taken into account in possible connections between the genesis of the study ZMP ridges and pits in a periglacial environment are lithalsas, or rather, remnant of collapsed lithalsas (Pissart, 2003). Lithalsas are permafrost mounds formed by ice segregation in mineral-rich soil (Wolfe et al., 2014; Calmels et al., 2008). They have an almost perfect circular or oval shape with diameters ranging from 30 to 90 m (50 m average) and are impounded by rim ridges of mineralogenic sediment (Calmels et al., 2008; Pissart, 2013; Demoulin et al., 2018; Ross et al., 2019). The remnants of lithalsa hollows always contain peat (Pissart, 2003). They are rounded on quasi-horizontal surfaces (<1°) and elongate on inclined surfaces (Demoulin et al., 2018). The density of such forms is high, but the lack of data makes it impossible to compare them with the studied forms. Lithalsas are too small and too uniform in size compared the ZMP ridges and pits, whose surfaces are also highly diverse (Figs. 7, 8) so therefor it is unlikely that the ridges and pits here are collapsed lithalsas.

**Table 2**
The main parameters of ridges and pits.

| Field | Sum of pits area [$m^2$] | Sum of ridges length [m] | Index density of ridge per $km^2$ | Percentage of pit area in the field | Aspect azimuth | Frequency of pits | Index density of pits per $km^2$ | Mean elongation ratio [E] | Field area [$m^2$] |
|---|---|---|---|---|---|---|---|---|---|
| A2 | 43,250.45 | 4708.95 | 18.84 | 17.30 | 167 | 48 | 192 | 1.62 | 250,000 |
| A1 | 27,352.73 | 4765.87 | 19.06 | 10.94 | 317 | 49 | 196 | 1.62 | 250,000 |
| B1 | 56,047.96 | 4615.57 | 18.46 | 22.42 | 322 | 52 | 208 | 1.80 | 250,000 |
| B3 | 89,751.95 | 4763.79 | 19.06 | 35.90 | 2 | 51 | 204 | 1.68 | 250,000 |
| B2 | 74,931.58 | 5306.21 | 21.22 | 29.97 | 354 | 57 | 228 | 1.63 | 250,000 |
| F1 | 122,229.86 | 3105.22 | 12.42 | 48.89 | 16 | 42 | 168 | 1.79 | 250,000 |
| E1 | 31,586.6 | 5279.95 | 21.12 | 12.63 | 351 | 46 | 184 | 1.68 | 250,000 |
| C1 | 69,764.83 | 4817.39 | 19.27 | 27.91 | 208 | 55 | 220 | 1.89 | 250,000 |
| C2 | 72,975.61 | 5063.5 | 20.25 | 29.19 | 226 | 66 | 264 | 1.72 | 250,000 |
| G1 | 52,263.81 | 6176.46 | 24.71 | 20.91 | 46 | 87 | 348 | 1.75 | 250,000 |
| D1 | 63,689.73 | 5323.3 | 21.29 | 25.48 | 305 | 69 | 276 | 1.69 | 250,000 |
| B4 | 108,033.17 | 4350.04 | 17.40 | 43.21 | 43 | 51 | 204 | 1.72 | 250,000 |
| G2 | 58,108.23 | 4938.6 | 19.75 | 23.24 | 81 | 66 | 264 | 1.75 | 250,000 |
| F2 | 89,827.09 | 4120.83 | 16.48 | 35.93 | 357 | 62 | 248 | 1.67 | 250,000 |

**Table 3**
Pit-parameters statistics.

| | Minimum | 1st quartile | Median | Mean | 3rd quartile | Maximum |
|---|---|---|---|---|---|---|
| Area ($m^2$) | 38.13 | 303.04 | 597.85 | 1435.42 | 1603.00 | 28,108.70 |
| Length (m) | 8.04 | 24.39 | 36.76 | 48.32 | 61.68 | 247.63 |
| Width (m) | 6.28 | 15.72 | 21.68 | 28.46 | 36.21 | 157.16 |
| Elongation ratio [E] | 1.03 | 1.32 | 1.58 | 1.72 | 1.97 | 4.60 |

*5.1.2. Glacial origin of ridges and pits*

Based on the arguments we present here and the morphology of the ZMP ridges and pits, we interpret the ridges and pits to have been made during downwasting of the Weichselian glacier margin. Zaleszkiewicz (2005a, 2005b) suggests that the ice retreat in the area occurred in a downwasting manner; this is supported by the presence of hummock forms and large kettle-holes associated with the melting of buried ice. The final melting of dead ice in the study area took place just at the intersection of the Preboreal–Boreal transition (Błaszkiewicz, 2011; Van Loon et al., 2012; Błaszkiewicz et al., 2015; Słowiński et al., 2015; Wojciechowski and Jonczak, 2023).

There are not many examples of glaciogenic forms reported in the literature that are analogous to the ZMP ridges and pits (Aartolahti, 1974; Lagerbäck, 1988; Mollard, 2000; Munro and Shaw, 1997; Knudsen et al., 2006; Clayton et al., 2008; Evans et al., 2007; Alexanderson et al., 2022). The ZMP ridges and pits are associated with the knob-and-kettle topography of hummocky moraine, which is composed of non-oriented, chaotically organized of hummocks (Eyles et al., 1999; Johnson and Clayton, 2003; Clayton et al., 2008). Hummocky moraine forms at ice-sheet margins, which in the study case had flowed upslope against underlying topographic obstacles (Clayton and Moran, 1974; Eyles et al., 1999; Evans and Evans, 2022) following large-scale ice surging (Alexanderson et al., 2022). Among the numerous features associated with hummock that are circular similar to the ZMP ridges and pits are doughnut-like rim ridges, linear ridges, kettle holes, Pulju mroaines, Veiki moraines, and ice-walled lake plains, all of which have curvilinear or circular relief (e.g., Benn, 1992; Ham and Attig, 1996; Eyles et al., 1999; Knudsen et al., 2006; Clayton et al., 2008; Evans et al., 2007; Alexanderson et al., 2022).

Pulju moraines are non-oriented, and their shape varied from semi-circular to arcuate ridges/moraine hummocks (Aartolahti, 1974; Johansson and Nenonen, 1989). Their widths vary from 30 to 100 m in Finnish Lapland (Sutinen et al., 2014).

Veiki moraines in northern Sweden are nearly circular elevated plateaus surrounded by ridges that are separated by pits (Lagerbäck, 1988; Alexanderson et al., 2022). This type of moraine consists of flat-topped mounds, often with rim ridges, and are interpreted commonly as pre-Late Weichselian ice-walled-lake plains covered by till of the most recent glaciation (Lagerbäck, 1988; Clayton et al., 2008; Sigfúsdóttir, 2013; Alexanderson et al., 2022; Allred et al., 2014). Veiki moraines are larger than Pulju moraines. Both are found in northern Finland and Sweden. Veiki moraine is morphologically and stratigraphically distinguished by the presence of overriding ice, such as occurs with weak drumlinisation (Lagerbäck, 1988). The ZMP ridges and pits do not surround plateau comprised of lake sediment.

As it is unlikely that the ridges and pits where formed in a periglacial environment, and because they occur within a proglacial position that is characterized by many landforms associated with 'hummocky moraine', 'stagnation moraine', or 'dead-ice moraine' terrain, we interpret these ridges and pits to have formed by the melting of stagnant ice that was rich in glacial debris. The study ZMP ridges and pits are distinguished by the fact that they do not form plateaux separated from each other by a flat surface; on the contrary, adjacent pits are separated from each other by a ridge. Moreover, they are generally ovoid, and sometimes even round (Figs. 4–6, 9–10). We suggest that this is an area of unique glacial relief whose origin is probably related to the ice sheet's stagnation, then its final disintegration here. We propose calling such glacial relief "ZMP ridges and pits".

Undoubtedly, the subglacial pre-Weichselian topography of the area played an important role by presenting a counterslope for the advancing ice sheet (Fig. 2). We suggest that the ridges and pits formed through the degradation of a stagnant ice-sheet front into blocks of dead ice. That ice in degradation divided into many blocks of very different sizes, although these were usually small or very small. Only in the case of compound pits did the large blocks begin to divide into smaller ones during progressive deglaciation (Gravenor and Kupsch, 1959); hence the traces of ridges can be found at pit bottoms (Figs. 9, 10). Pit density ($D_D$) (Table 2) indicates that the ice surface must have had very high crevasse density. Forms such as crevasses may be indicative of the influence of previous live ice, which are described as 'controlled'. Such control can be provided by fractures and thrust planes that respond to the stresses acting in the live ice (Gravenor and Kupsch, 1959). This finding may be linked to surge-type ice-mass dynamics because: 1) surging glaciers commonly contain a complex system of crevasses (Ben-Yehoshua et al., 2023; Van Wyk de Vries et al., 2023); and 2) surging glaciers (Clayton et al., 1985) can create abundant supraglacial debris that could provide ridge-building material. Moreover, we compare the pit orientations with the expected stress directions of the surging glacier to check if the ridge and

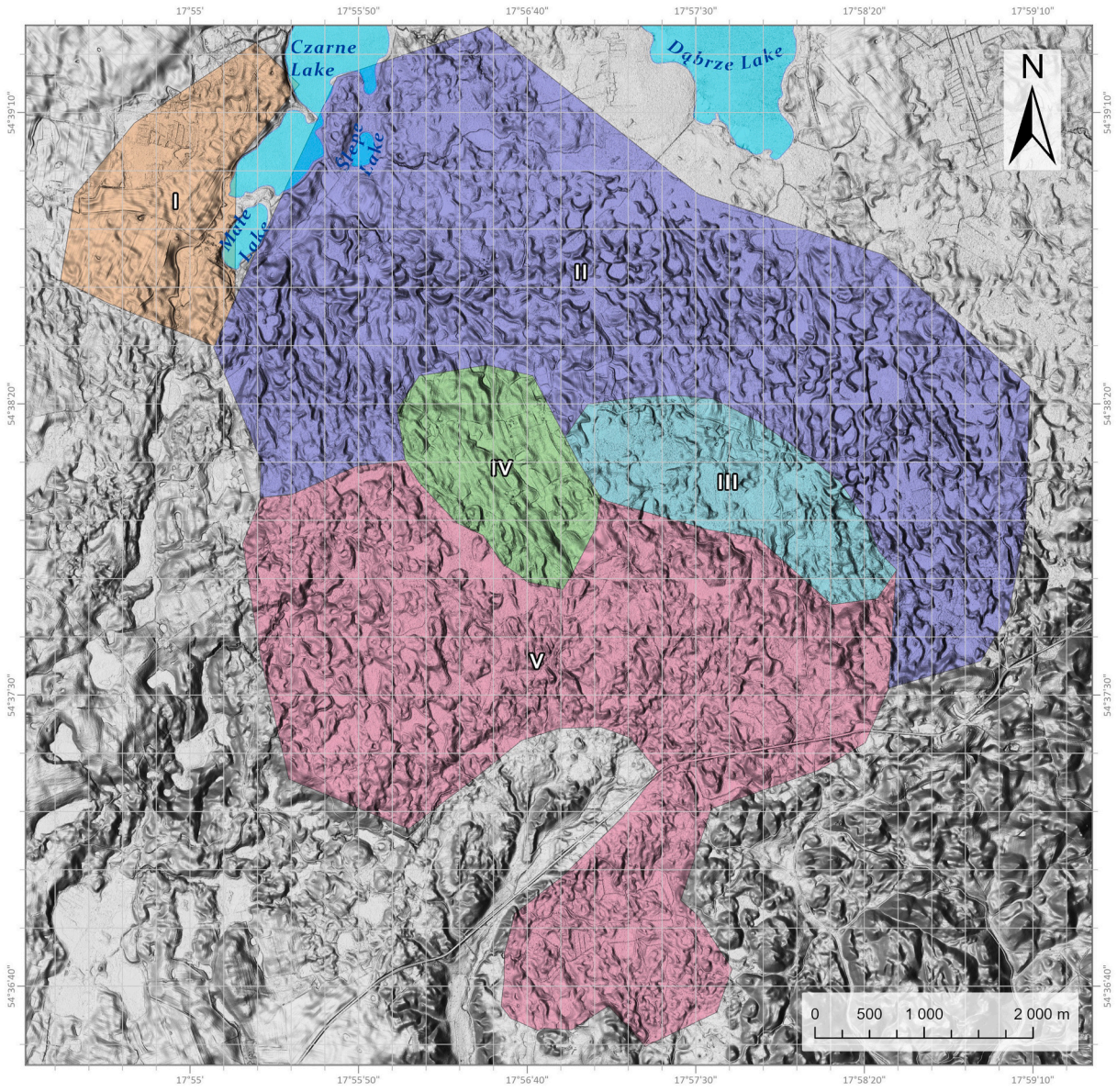


**Fig. 15.** Division of studied area into zones (I-V) based on topographical diversity of ridges and pits.

pit system could be crevasse related. Crevasses tend to develop wherever tensile stresses exceed the strength of ice (Vornberger and Whillans, 1990; Benn and Evans, 2010) and are always oriented at right angles to the stress direction. Also, where lateral shear acts, longitudinal crevasses are approximately oriented parallel to the direction of ice flow and at an angle of 45° (Benn and Evans, 2010; Christoffersen et al., 2005; Evans et al., 2007; Kjær et al., 2008; Colgan et al., 2016; Jennings and Hambrey, 2021; Van Wyk de Vries et al., 2023). It has been shown that these nearly vertical crevasses can extend from the base of the ice to the surface (Evans and Rea, 1999; Johnson et al., 2010). Crevasses can vary in scale, from metres long in valley glaciers and glacial cirques to tens of kilometres long at the margins of the Antarctic Ice Sheet (Van Wyk de Vries et al., 2023). A reconstruction of fracture orientation in the ice sheet covering the Żarnowiec Moraine Plateau is crucial to understanding if such a ridge system can be explained by a hypothetical crevasse system. However, the system of crevasses was most likely very complicated and may also have changed over time (Van Wyk de Vries et al., 2023).

The study area's ice sheet most likely advanced from the north or north-north-west. Crevasses perpendicular to the movement of the ice sheet correlate with this direction (Benn and Evans, 2010; Christoffersen et al., 2005; Evans et al., 2007; Kjær et al., 2008; Jennings and Hambrey, 2021; Van Wyk de Vries et al., 2023). A crevasse fill origin is strengthened because the expected crevasse orientations in the ice, based on ice-flow directions, are similar to the orientation of the ridges. This direction is evident in test fields B1 and B2 in the most northern part of study area, expressed as L-axes orientation pits at N70–80E. On the eastern site/slope of the plateau, the ice sheet has adapted to its instream obstacle, as indicated by the direction of the N10-20E L-axis pits in test fields F2, G1, and G2 (Fig. 14). The presence of the obstacle also resulted in tensile stresses and extensional movement of the ice. The orientation of the longer axis of the pits (L) shows that the direction of these tensile stresses, along with extensional movement, is parallel to the NNW–SSE direction of ice movement. This orientation is recorded in the western test fields C1 and C2 (zone V) and in the eastern fields B3 and B4 (zone II), and is perpendicular to the general slope angle in these zones (Figs. 14, 15). The speed of this ice must have been greater than that of the ice crossing the obstacle. At the boundary between faster and slower flowing ice, crevasses may have formed obliquely to the preceding ones (Jennings and Hambrey, 2021; Van Wyk de Vries et al., 2023). In test

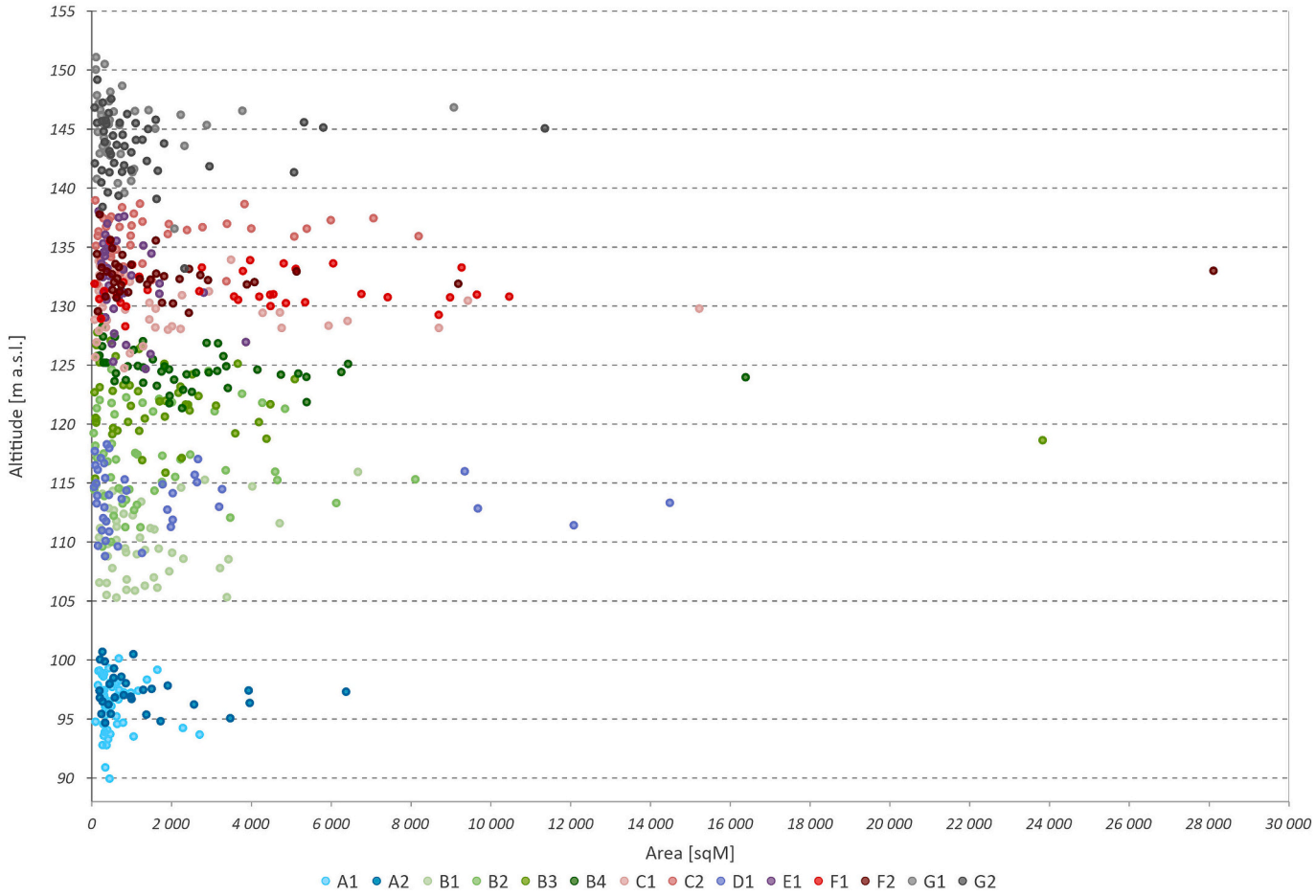


**Fig. 16.** Size diversity of pits depending on location above sea level.

fields C1 and C2, they are marked by the direction of the longer axis of pits (L) being oriented NNW–SSE. This system is oriented at ~10–30° to the N–S-oriented crevasses (Fig. 14). They may represent Chevron-type crevasses, which are oriented obliquely up-glacier because of shear stresses acting at the glacier's margins (Jennings and Hambrey, 2021). The obtained results show how complex the crevasse system was in this area. Moreover, the spatial density of crevasses and the associated ridges very much remain to be understood. Research to date shows that some glaciers and ice sheets have high density of crevasses. Examples include two glaciers in Trygghamna on Western Svalbard (Ben-Yehoshua et al., 2023), Eyjabakkajokull glacier in eastern Iceland (Lamsters et al., 2022) and Narsap Sermia glacier (Van Wyk de Vries et al., 2023) or the Store Glacier in Greenland (Chudley et al., 2021). In many cases, their very high density of crevasses are associated with surge-type glaciers or rapid and extensional ice flow (Benn and Evans, 2010; Ben-Yehoshua et al., 2023). This same phenomenon may account for the creation of a system of crevasses and the associated complex of ramparted depressions as expressed on the Żarnowiec Moraine Plateau (Fig. 2).

## 6. Conclusions

Detailed morphometric analyses of ridges and pits in the Żarnowiec Moraine Plateau (N Poland) facilitates the following conclusions:

a) Ridges and pits are characterized by great diversity. Specifically, they form a very dense network of forms of various sizes that are roughly circular and diversely oriented. Most of them are linked to each other in a step-wise fashion. The pits are surrounded by ridges of various widths and heights. Large forms are referred to as "compound pits".
b) Their diverse morphometry allowed us to distinguish five zones (I—V) covering different parts of the morainal plateau. Each zone has its own distinct set of characteristics that mark the development of its ridges and pits system. This distinction includes the inclination of the slopes (Fig. 2), the density of the studied forms, and—above all—the orientation of the longer axis of the pits (L) (Fig. 14). The fields also differ in their a.s.l. position (Fig. 16).
c) The morphometric parameters of the study forms compare with forms from various morphogenetic zones as reported elsewhere, indicating that they can be associated with a past glacial environment.
d) The formation of such glacial relief is related to the ice sheet having been particularly high crevasses density in this area along with the division of dead ice into blocks of various sizes. A surge-type ice mass experienced progressive deglaciation, forming pits. These pits were subsequently transformed through organic-sediment infill. The substantial cracking of the ice was the result of the ice sheet crossing a large terrain obstacle that constituted a counterslope for a advancing ice sheet. The complex crevasse system consisted of fractures perpendicular to ice flow, parallel ones related to tensile stresses in association with extensional ice movement, and Chevron-type crevasses that were oriented obliquely up-glacier, being related to differences in speed between ice masses crossing and flowing around an obstacle.
e) Ridges and pits in the study area create a special type of hummocky moraine. Due to the specificity of the study forms and their very high spatial density, which is incomparable to other forms of this type

occurring in a glacial environment, we propose to call this type of glacial relief "ZMP ridges and pits."

## Funding

This research was funded by project No. 2022/45/B/ST10/03167 of the National Science Centre, Poland. Professor Mirosław Błaszkiewicz is the head of this grant.

## CRediT authorship contribution statement

**Barbara Woronko:** Writing – review & editing, Writing – original draft, Visualization, Validation, Methodology, Investigation, Formal analysis, Conceptualization. **Weronika Danel:** Writing – review & editing, Writing – original draft, Visualization, Validation, Methodology, Investigation, Formal analysis, Conceptualization. **Mirosław Błaszkiewicz:** Writing – review & editing, Writing – original draft, Investigation, Conceptualization. **Piotr Hermanowski:** Writing – review & editing, Writing – original draft, Methodology, Investigation, Conceptualization. **Olaf Juschus:** Writing – review & editing, Writing – original draft, Investigation. **Mateusz Kramkowski:** Writing – review & editing, Investigation. **Bruno Garrett:** Writing – review & editing, Visualization, Investigation. **Achim Brauer:** Writing – review & editing, Investigation.

## Declaration of competing interest

The authors declare that they have no known competing financial interests or personal relationships that could have appeared to influence the work reported in this paper.

## Data availability

All data to reproduce the work in the paper are available in the repository https://doi.org/10.5281/zenodo.10694177 (Woronko et al., 2024).

## Acknowledgements

We would like to thank the Choczewo Forest District and the foresters in the Brodnica and Dąbrówka Forest Districts for their help with fieldwork. We thank student Jakub Umięcki (Nicolaus Copernicus University, Toruń) for the support morphometric analysis of the study forms. We would like to thank the Mark D. Johnson from Department of Earth Sciences University of Gothenburg for careful reviews, which helped improve the quality of the paper. We thank an anonymous reviewer for careful reading of the manuscript and constructive remarks.

## References

Aartolahti, T., 1974. Ring ridge hummocky moraines in northern Finland. Fennia 134, 1–21.

Adamczyk, A., Wysota, W., Piotrowski, J.A., 2022. Inventory of glacial curvilineations (GCLs) at the southern periphery of the last Scandinavian Ice Sheet. Geomorphology 400, 108094. https://doi.org/10.1016/j.geomorph.2021.108094.

Alexanderson, H., Hättestrand, M., Lindqvist, M.A., Sigfúsdóttir, T., 2022. MIS 3 age of the Veiki moraine in N Sweden–dating the landform record of an intermediate-sized ice sheet in Scandinavia. AAAR, 54(1), 239–261. doi:https://doi.org/10.1080/15230430.2022.2091308.

Allred, K., Luo, W., Konen, M., Curry, B.B., 2014. Morphometric analysis of ice-walled lake plains in Northern Illinois: implications of lake elongation by wind-induced dual-cycle currents. Geomorphology 220, 50–57. https://doi.org/10.1016/j.geomorph.2014.05.022.

Benn, D.I., 1992. The genesis and significance of 'hummocky moraine': evidence from the Isle of Skye, Scotland. Quat. Sci. Rev. 11, 781–799. https://doi.org/10.1016/0277-3791(92)90083-K.

Benn, D.I., Evans, D.J.A., 2010. Glaciers and Glaciation, 2nd edition. Routledge, London. https://doi.org/10.4324/9780203785010.

Ben-Yehoshua, D., Aradóttir, N., Farnsworth, W.R., Benediktsson, Í.Ö., Ingólfsson, Ó., 2023. Formation of crevasse-squeeze ridges at Trygghamna. Svalbard. Earth Surf. Process. Landf. 48 (12), 2334–2348. https://doi.org/10.1002/esp.5631.

Błaszkiewicz, M., 2011. Timing of the final disappearance of permafrost in the central European Lowland, as reconstructed from the evolution of lakes in N Poland. Geol. Quarterly 55 (4), 361–374. https://gq.pgi.gov.pl/article/view/7694.

Błaszkiewicz, M., Danel, W., 2019. Formy pierścieniowe w rejonie Wejherowa jako prawdopodobne pozostałości po-pingo i ich znaczenie dla paleogeografii późnego glacjału w północnej Polsce. Ring forms in the area of Wejherowo as likely remnants of pingos, and their significance for Late-Glacial paleogeography in Northern Poland. Przegląd Geog. 91 (3), 405–419. https://rcin.org.pl/publication/108233.

Błaszkiewicz, M., Piotrowski, J., Brauer, A., Gierszewski, P., Kordowski, J., Kramkowski, M., Lamparski, P., Lorenz, S., Noryśkiewicz, A., Ott, F., Słowiński, M., Tyszkowski, S., 2015. Climatic and morphological controls on diachronous postglacial lake and river valley evolution in the area of Last Glaciation, northern Poland. Quat. Sci. Rev. 109, 13–27. https://doi.org/10.1016/j.quascirev.2014.11.023.

Boone, S.J., Eyles, N., 2001. Geotechnical model for great plains hummocky moraine formed by till deformation below stagnant ice. Geomorphology 38 (1–2), 109–124. https://doi.org/10.1016/S0169-555X(00)00072-6.

Calmels, F., Allard, M., Delisle, G., 2008. Development and decay of a lithalsa in Northern Quebec: a geomorphological history. Geomorphology 97 (3–4), 287–299. https://doi.org/10.1016/j.geomorph.2007.08.013.

Chandler, B.M., Lovell, H., Boston, C.M., Lukas, S., Barr, I.D., Benediktsson, Í.Ö., Benn, D. I., Clark, Ch.D., Darvill, Ch.M., Evans, D.J.A., Ewertowski, M.W., Loibl, D., Margold, M., Otto, J-Ch., Roberts, D.H., Stokes, Ch.R., Storrar, R.D., Stroeven, A.P., 2018. Glacial geomorphological mapping: a review of approaches and frameworks for best practice. Earth Sci. Rev. 185, 806–846. https://doi.org/10.1016/j.earscirev.2018.07.015.

Chiba, T., Kaneta, S., Suzuki, Y., 2008. Red relief image map: new visualization method for three dimensional data, Remote Sens. Spat. Inf. Sci. 37.

Christoffersen, P., Piotrowski, J.A., Larsen, N.K., 2005. Basal processes beneath an Arctic glacier and their geomorphic imprint after a surge, Elisebreen, Svalbard. Quat. Res. 64 (2), 125–137. https://doi.org/10.1016/j.yqres.2005.05.009.

Chudley, T.R., Christoffersen, P., Doyle, S.H., Dowling, T.P.F., Law, R., Schoonman, C.M., Bougamont, M., Hubbard, B., 2021. Controls on water storage and drainage in crevasses on the Greenland ice sheet. J. Geophysical Research: Earth Sur. 126 (9), e2021JF006287. https://doi.org/10.1029/2021JF006287.

Clayton, L., Moran, S.R., 1974. A glacial process-form model. In: Glacial Geomorphology: A Proceedings Volume of the Fifth Annual Geomorphology Symposia Series, Held at Binghamton New York September 26–28. Springer Netherlands, Dordrecht, pp. 89–119.

Clayton, L., Teller, J.T., Attig, J.W., 1985. Surging of the southwestern part of the Laurentide Ice Sheet. Boreas 14, 235–241.

Clayton, L., Attig, J.W., Ham, N.R., Johnson, M.D., Jennings, C.E., Syverson, K.M., 2008. Ice-walled-lake plains: implications for the origin of hummocky glacial topography in middle North America. Geomorphology 97, 237–248. https://doi.org/10.1016/j.geomorph.2007.02.045.

Colgan, W., Rajaram, H., Abdalati, W., McCutchan, C., Mottram, R., Moussavi, M.S., Grigsby, S., 2016. Glacier crevasses: observations, models, and mass balance implications. Rev. Geophys. 54 (1), 119–161. https://doi.org/10.1002/2015RG000504.

Dąbrowski, A., Jasiewicz, J., 2014. Zastosowanie form morfometrycznych do analizy zróżnicowania wybranych typów powierzchni na obszarach młodoglacjalnych. Badania Fizjograficzne R. V – Seria A – Geografia Fizyczna 65, 95–111. https://doi.org/10.14746/bfg.2014.5.8.

Danel, W., Borecka, A., 2020. Geological Map of Poland 1:200 000, sheet A: (6) Słupsk, 2nd edition. Polish Geological Institute – National Research Institute, Warsaw, Poland. https://bazadata.pgi.gov.pl/data/mgp200/mapy/edycja2/mgp200A06-edycja2.jpg. (Accessed 1 March 2024).

Daxer, C., 2020. Topographic openness maps and Red relief image maps in QGIS. Technol. Rep. Inst. Geol 17, 1–15. https://doi.org/10.13140/RG.2.2.18958.31047.

Demoulin, A., Juvigné, E., Houbrechts, G., 2018. The periglacial ramparted depressions of the Hautes Fagnes Plateau: traces of Late Weichselian lithalsas. Landscapes and Landforms of Belgium and Luxembourg 101–113. https://doi.org/10.1007/978-3-319-58239-9_7.

Dzieduszyńska, D.A., Petera-Zganiacz, J., 2018. Small-scale geologic evidence for Vistulian decline cooling periods: case studies from the Łódź Region (Central Poland). Bull. Geol. Soc. Finl. 90 (2), 41–54.

Evans, D.J., Evans, I.S., 2022. Glacial processes and landforms. Geol. Soc. Lond. Mem. 58, 333–377. https://doi.org/10.1144/M58-2021-17.

Evans, D.J.A., Rea, B.R., 1999. The geomorphology and sedimentology of surging glaciers: a landsystems approach. Ann. Glaciol. 28, 75–82. https://doi.org/10.3189/172756499781821823.

Evans, D.J.A., Twigg, D.R., Rea, B.R., Shand, M., 2007. Surficial geology and geomorphology of the Brúarjökull surging glacier landsystem. J. Maps 3 (1), 349–367. https://doi.org/10.1080/jom.2007.9710850.

Eyles, N., Boyce, J.I., Barendregt, R.W., 1999. Hummocky moraine: sedimentary record of stagnant Laurentide Ice Sheet lobes resting on soft beds. Sediment. Geol. 123 (3–4), 163–174. https://doi.org/10.1016/S0037-0738(98)00129-8.

French, H.M., 2017. The Periglacial Environment, fourth ed. John Wiley & Sons Ltd, Hoboken, NJ, ISBN 978-1-119-13278-3, p. 515.

French, H.M., Dimitroff, M., 2001. Cold-climate origin of the enclosed depressions and wetlands ('spungs') of the Pine Barrens, Southern New Jersey, USA. Permafr. Periglac. Process. 12, 337–350. https://doi.org/10.1002/ppp.401.

Gravenor, C.P., Kupsch, W.O., 1959. Ice-disintegration features in western Canada. J. Geol. 67 (1), 48–64.

Greenwood, S.L., Hughes, A.L., Avery, R.S., 2023. Fennoscandia: glacial landforms during initial deglaciation (18.9–14.6 ka). In: European Glacial Landscapes. Elsevier, pp. 85–94.
Grosse, G., Jones, B.M., 2011. Spatial distribution of pingos in northern Asia. Cryosphere 5 (1), 13–33. https://doi.org/10.5194/tc-5-13-2011.
Hallet, B., 2013. Stone circles: form and soil kinematics. Philosophical Transactions of the Royal Society A: Math. Phys. Eng. Sci. 371, 20120357. https://doi.org/10.1098/rsta.2012.0357.
Ham, N.R., Attig, J.W., 1996. Ice wastage and landscape evolution along the southern margin of the Laurentide Ice Sheet, northcentral Wisconsin. Boreas 25, 171–186. https://doi.org/10.1111/j.1502-3885.1996.tb00846.x.
Höfle, B., Mandlburger, G., Pfeifer, N., Rutzinger, M., Bell, R.H.V., 2009. Potential of airborne LiDAR in geomorphology-a technological perspective. In. Geophys. Res. Abstr. 11. http://meetingorganizer.copernicus.org/EGU2009/EGU2009-4630.pdf. (Accessed 1 March 2024).
Jasiewicz, J., Stepinski, T.F., 2013. Geomorphons — a pattern recognition approach to classification and mapping of landforms. Geomorphology 182, 147–156. https://doi.org/10.1016/j.geomorph.2012.11.005.
Jennings, S.J.A., Hambrey, M.J., 2021. Structures and deformation in glaciers and ice sheets. Rev. Geophys. 59, 3. https://doi.org/10.1029/2021RG000743.
Johansson, P., Nenonen, J., 1989. Till stratigraphical studies in the Pulju area in northern Finland. Geological Survey of Finland, Current Research 1990, 131–134. https://tupa.gtk.fi/julkaisu/specialpaper/sp_012_pages_131_134.pdf. (Accessed 1 March 2024).
Johnson, M.D., Clayton, L., 2003. Supraglacial landsystems in lowland terrain. In: Evans, D. (Ed.), Glacial Landsystems. Arnold, London, pp. 228–258. https://doi.org/10.4324/9780203784976.
Johnson, M.D., Mickelson, D.M., Clayton, L., Attig, J.W., 1995. Composition and genesis of glacial hummocks, western Wisconsin. Boreas 24, 97–116.
Johnson, M.D., Schomacker, A., Benediktsson, Í.Ö., Geiger, A.J., Ferguson, A., Ingólfsson, Ó., 2010. Active drumlin field revealed at the margin of Múlajökull, Iceland: a surge-type glacier. Geology 38 (10), 943–946. https://doi.org/10.1130/G31371.1.
Jones, B.M., Grosse, G., Hinkel, K.M., Arp, C.D., Walker, S., Beck, R.A., Galloway, J.P., 2012. Assessment of pingo distribution and morphometry using an IfSAR derived digital surface model, western Arctic Coastal Plain. Northern Alaska. Geomorphology 138 (1), 1–14. https://doi.org/10.1016/j.geomorph.2011.08.007.
Jorge, M.G., Brennand, T.A., 2017. Measuring (subglacial) bedform orientation, length, and longitudinal asymmetry – method assessment. PLoS One 12 (3), e0174312. https://doi.org/10.1371/journal.pone.0174312.
Karasiewicz, T., Hrynowiecka, A., Weckwerth, P., Tobojko, L., Pawłowski, D., Wysota, W., Krawiec, A., Dąbrowski, M., 2023. Origin and post-glacial evolution of surface cracks: a case study from the area of the Last Glaciation, north-eastern Poland. Earth Surf. Process. Landf. 49 (2), 525–548. https://doi.org/10.1002/esp.5719.
Kjær, K.H., Korsgaard, N.J., Schomacker, A., 2008. Impact of multiple glacier surges-a geomorphological map from Brúarjökull. East Iceland, J. Maps 4 (1), 5–20. https://doi.org/10.4113/jom.2008.91.
Knudsen, C.G., Larsen, E., Sejrup, H.P., Stalsberg, K., 2006. Hummocky moraine landscape on Jæren, SW Norway—implications for glacier dynamics during the last deglaciation. Geomorphology 77 (1–2), 153–168. https://doi.org/10.1016/j.geomorph.2005.12.011.
Kokalj, Ž., Hesse, R., 2017. Air borne Laser Scanning Raster Data Visualization. A Guide to Good Practice, vol. 14. Prostor, Kraj, Čas, p. 5. https://doi.org/10.3986/9789612549848.
Kozarski, S., 1986. Early Vistulian permafrost occurence in north-west Poland. Biul. Peryglac. 31, 163–170.
Kozarski, S., 1991. Upper Plenivistulian deglaciation and expansion of the periglacial zone in NW Poland. In: Abstracts Symposium Periglacial Environments in Relation to Climatic Change (Maastricht/Amsterdam, 3rd-6th May 1991). Vrije Universiteit Amsterdam, p. 24.
Lagerbäck, R., 1988. The Veiki moraines in northern Sweden – widespread evidence of an Early Weichselian deglaciation. Boreas 17, 469–486. https://doi.org/10.1111/j.1502-3885.1988.tb00562.x.
Lamsters, K., Ješkins, J., Sobota, I., Karušs, J., Džeriņš, P., 2022. Surface characteristics, elevation change, and velocity of high-arctic valley glacier from repeated high-resolution UAV photogrammetry. Remote Sens. 14 (4), 1029. https://doi.org/10.3390/rs14041029.
Lindqvist, M.A., 2020. Kortejärvi Veiki Moraine Plateau - A Key to the Glacial History of Northern Sweden. UiT the Arctic University of Norway. https://hdl.handle.net/10037/18227. (Accessed 1 March 2024) (MSc Thesis 109).
Lindsay, J.B., 2016. Whitebox GAT: a case study in geomorphometric analysis. Comput. Geosci. 95, 75–84. https://doi.org/10.1016/j.cageo.2016.07.003.
Łopuch, M., Sokołowski, R.J., Jary, Z., 2023. Factors controlling the development of cold-climate dune fields within the central part of the European Sand Belt–insights from morphometry. Geomorphology, 420, 108514. doi:https://doi.org/10.1016/j.geomorph.2022.108514.
Marks, L., Bitinas, A., Błaszkiewicz, M., Börner, A., Guobyte, R., Rinterknecht, V., Tylmann, K., 2023. Chapter 11: Northern Central Europe: glacial landforms during deglaciation (18.9–14.9 ka). In: Palacios, D., Hughes, P.D., García-Ruiz, J.M., Andrés, N. (Eds.), European Glacial Landscapes: Last Deglaciation. Elsevier, Amsterdam, pp. 95–104. https://doi.org/10.1016/C2021-0-00331-X.
Mollard, J.D., 2000. Ice-shaped ring-forms in Western Canada: their airphoto expressions and manifold polygenetic origins. Quat. Int. 68–71, 187–198. https://doi.org/10.1016/s1040-6182(00)00043-4.
Munro, M., Shaw, J., 1997. Erosional origin of hummocky terrain in south-central Alberta. Canada. Geology 25 (11), 1027–1030.
Nagi, R., 2014. Multi-directional hillshade makes your maps pop. ArcUser Fall. 17 (4). https://www.esri.com/about/newsroom/arcuser/multi-directional-hillshade-makes-your-maps-pop/. (Accessed 1 March 2024).
Ojala, A.E., Peterson, G., Mäkinen, J., Johnson, M.D., Kajuutti, K., Palmu, J.P., Ahokangas, E., Öhrling, C., 2019. Ice sheet scale distribution of unique triangular-shaped hummocks (murtoos) – a subglacial landform produced during rapid retreat of the Scandinavian Ice Sheet. Ann. Glaciol. 60, 115–126. https://doi.org/10.1017/aog.2019.34.
Ojala, A.E., Mäkinen, J., Ahokangas, E., Kajuutti, K., Valkama, M., Tuunainen, A., Palmu, J.P., 2021. Diversity of murtoos and murtoo-related subglacial landforms in the Finnish area of the Fennoscandian Ice Sheet. Boreas 50 (4), 1095–1115. https://doi.org/10.1111/bor.12526.
Paulen, R.C., McClenaghan, M.B., 2015. Late Wisconsin ice-flow history in the Buffalo Head Hills kimberlite field, north-central Alberta. Can. J. Earth Sci. 52 (1), 51–67. https://doi.org/10.1139/cjes-2014-0109.
Petera-Zganiacz, J., Dzieduszyńska, D.A., 2017. Palaeoenvironmental proxies for permafrost presence during the Younger Dryas, central Poland. Permafr. Periglac. 28 (4), 726–740. https://doi.org/10.1002/ppp.1956.
Peterson, G., Johnson, M.D., 2021. Sedimentology and internal structure of murtoos - V-shaped landforms indicative of a dynamic subglacial hydrological system. Geomorphology 380, 107644. https://doi.org/10.1016/j.geomorph.2021.107644.
Peterson, G., Johnson, M., Smith, C., 2017. Glacial geomorphology of the south Swedish uplands – focus on the spatial distribution of hummock tracts. J. Maps 13 (2), 534–544. https://doi.org/10.1080/17445647.2017.1336121.
Pissart, A., 2002. Palsas, lithalsas and remnants of these periglacial mounds. A progress report. Prog. Phys. Geogr. 26 (4), 605–621. https://doi.org/10.1191/0309133302pp354ra.
Pissart, A., 2003. The remnants of Younger Dryas lithalsas on the Hautes Fagnes Plateau in Belgium and elsewhere in the world. Geomorphology 52 (1–2), 5–38. https://doi.org/10.1016/S0169-555X(02)00246-5.
Pissart, A., 2013. Palsas and lithalsas. Treatise on Geomorphology 8 (16). https://doi.org/10.1016/B978-0-12-374739-6.00210-4.
Rinterknecht, V., Börner, A., Bourlès, D., Braucher, R., 2014. Cosmogenic 10Be dating of ice sheet marginal belts in Mecklenburg-Vorpommern, Western Pomerania (northeast Germany). Quat. Geochronol. 19 (42–51), 1871-1014. https://doi.org/10.1016/j.quageo.2013.05.003.
Ross, N., Brabham, P., Harris, C., 2019. The glacial origins of relict 'pingos', Wales, UK. Ann. Glaciol. 60 (80), 138–150. https://doi.org/10.1017/aog.2019.40.
Sigfúsdóttir, Þ., 2013. A sedimentological and stratigraphical study of Veiki moraine in northernmost Sweden. In: Dissertations in Geology. Lund University.
Słowiński, M., Błaszkiewicz, M., Brauer, A., Noryśkiewicz, B., Ott, F., Tyszkowski, S., 2015. The role of melting dead ice on landscape transformation in the early Holocene in Tuchola Pinewoods, North Poland. Quat. Int. 388, 64–75. https://doi.org/10.1016/j.quaint.2014.06.018.
Smith, M.J., Clark, C.D., 2005. Methods for the visualization of digital elevation models for landform mapping. Earth Surf. Process. Landf. 30, 885–900. https://doi.org/10.1002/esp.1210.
Sookhan, S., Eyles, N., Bukhari, S., Paulen, R.C., 2021. LiDAR-based quantitative assessment of drumlin to mega-scale glacial lineation continuums and flow of the paleo Seneca-Cayuga paleo-ice stream. Quat. Sci. Rev. 263, 107003. https://doi.org/10.1016/j.quascirev.2021.107003.
Stager, J.K., 1956. Progress report on the analysis of the characteristics and distribution of pingos east of the mackenzie delta 1. Canadian Geographer/Le Géographe canadien 2 (7), 13–20. https://doi.org/10.1111/j.1541-0064.1956.tb01850.x.
Štular, B., Lozić, E., Eichert, S., 2021. Airborne LiDAR-derived digital elevation model for archaeology. Remote Sens. 13 (9), 1855. https://doi.org/10.3390/rs13091855.
Sutinen, R., 1992. Glacial Deposits, Their Electrical Properties and Surveying by Image Interpretation and Ground Penetrating Radar. BGSF (359 123 pp.).
Sutinen, R., Hyvönen, E., Middleton, M., Ruskeeniemi, T., 2014. Airborne LiDAR detection of postglacial faults and Pulju moraine in Palojärvi, Finnish Lapland. Glob. Planet. Chang. 115, 24–32. https://doi.org/10.1016/j.gloplacha.2014.01.007.
Szuman, I., Kalita, J.Z., Diemont, C.R., Livingstone, S.J., Clark, C.D., Margold, M., 2023. Evaluation of the role of the Baltic depression during deglaciation of the last Scandinavian Ice Sheet; a landform-driven investigation. Cryosphere Discuss. 1–29. https://doi.org/10.5194/tc-2023-107.
Tylmann, K., Rinterknecht, V.R., Woźniak, P.P., Bourlès, D., Schimmelpfennig, I., Guillou, V., ASTER Team, 2019. The Local Last Glacial Maximum of the southern Scandinavian Ice Sheet front: Cosmogenic nuclide dating of erratics in northern Poland. Quat. Sci. Rev. 219, 36–46. https://doi.org/10.1016/j.quascirev.2019.07.004 (ISSN 0277-3791).
Tylmann, K., Rinterknecht, V.R., Woźniak, P.P., Guillou, V., ASTER Team, 2022. Asynchronous dynamics of the last Scandinavian Ice Sheet along the Pomeranian ice-marginal belt: a new scenario inferred from surface exposure 10Be dating. Quat. Sci. Rev. 294, 107755. https://doi.org/10.1016/j.quascirev.2022.107755.
Van Loon, A.J., Błaszkiewicz, M., Degórski, M., 2012. The role of permafrost in shaping the Late Glacial relief of northern Poland. Neth. J. Geosci. 91 (1–2), 223–231. https://doi.org/10.1017/S001677460000161X.
Van Wyk de Vries, M., Lea, J.M., Ashmore, D.W., 2023. Crevasse density, orientation and temporal variability at Narsap Sermia. Greenland. J. Glaciol 69 (277), 1125–1137. https://doi.org/10.1017/jog.2023.3.
Vornberger, P.L., Whillans, I.M., 1990. Crevasse deformation and examples from ice stream B. Antarctica. J. Glaciol 36, 3–10. https://doi.org/10.3189/S0022143000005487.
Watson, E., 1975. Remains of round and linear pingos in the Cledlyn and Cletwr basins. In: Co-Ordinating Committee for Periglacial Research. Working group of the International Geographical Union Symposium: Guide to field excursion.

Wojciechowski, A., Jonczak, J., 2023. The record of geochemical changes in the biogenic-calcareous sediments of a kettle-hole in a young glacial landscape (western Kashubian Lakeland, North Poland). Studia Quat. 41–56. https://doi.org/10.24425/sq.2023.148031.

Wolfe, S.A., Stevens, C.W., Gaanderse, A.J., Oldenborger, G.A., 2014. Lithalsa distribution, morphology and landscape associations in the Great Slave Lowland, Northwest Territories, Canada. Geomorphology 204, 302–313. https://doi.org/10.1016/j.geomorph.2013.08.014.

Wolfe, S.A., Morse, P.D., Behnia, P., 2021. Spatial distribution of pingos in the Tuktoyaktuk coastlands and adjacent areas, Northwest Territories. Geological Survey of Canada. Open File 8787 (1). https://doi.org/10.4095/328305.

Woronko, B., Dąbski, M., 2023. The North European Plain. In: Oliva, M., Nývlt, D., Fernández-Fernández, J.M. (Eds.), Periglacial Landscapes of Europe. Springer, pp. 281–320.

Woronko, B., Danel, W., Błaszkiewicz, M., Hermanowski, P., Juschus, O., Kramkowski, M., Garrett, B., Brauer, A., 2024. Ramparted depressions in the Żarnowiec Moraine Plateau (N Poland). Zenodo. https://doi.org/10.5281/zenodo.10694177.

Yokoyama, R., Shirasawa, M., Pike, R.J., 2002. Visualizing topography by openness: A new application of image processing to digital elevation models. Photogramm. Eng. Remote Sensing 68 (3), 257–266.

Zaleszkiewicz, L., 2005a. Detailed Geological Map of Poland 1:50 000. sheet Łęczyce 13. Polish Geological Institute – National Research Institute, Warsaw, Poland. https://baza.pgi.gov.pl/resources.html?type=smgp&id=13.

Zaleszkiewicz, L., 2005b. Explanatory Text to the Detailed Geological Map of Poland 1: 50 000. Sheet Łęczyce 13. Polish Geological Institute – National Research Institute, Warsaw, Poland. https://baza.pgi.gov.pl/resources.html?type=smgp&id=13 (in Polish).